Electronic Supplementary Information (ESI)

Donor-Acceptor Covalent Organic Frameworks Propel Oxygen Reduction Reaction with Push-Pull Dynamics

Greesh Kumar[a], Sabuj Kanti Das [a,b], Thakur Rochak Kumar Rana[c], Surajit Samui[a], Laurent Billon[b], and Ramendra Sundar Dey [a]*

[a]*Institute of Nano Science and Technology, Sector- 81, Mohali-140306, Punjab, India.*

[b]*Bio-inspired Materials Group : Functionalities & Self-assembly, Universite de Pau et des Pays de l'Adour, E2S UPPA, UPPA/CNRS, IPREM UMR 5254, 2, Avenue du Président Angot, 64053 Pau, France.*
[c]*Department of Chemistry, Indian Institute Institute of Technology, Powai, Mumbai-400076, India.*

Email: rsdey@inst.ac.in

	and N1s Spectra
Fig. S12	Full survey of XPS analysis of TPB_TPA_COF catalyst and deconvoluted C1s and N1s Spectra
Fig. S13	PSD spectra of the TPA_TPT_COF catalyst material
Fig. S14	BET adsorption desorption isotherm and PSD spectra of the TPT_TPB_COF catalyst material
Fig. S15	BET adsorption desorption isotherm and PSD spectra of the TPB_TPA_COF catalyst material
Fig. S16	Electrical sheet resistance measurement (i–v) curve of TPA_TPT_COF, TPT_TPB_COF and TPB_TPA_COF catalysts
Fig. S17	Electrochemical active surface area analysis of TPA_TPT_COF, TPT_TPB_COF and TPB_TPA_COF materials
Fig. S18	Electrochemical impedance spectroscopy (EIS) spectra of TPA_TPT_COF, TPT_TPB_COF, TPB_TPA_COF and equivalent fitted circuit.
Fig. S19	Linear sweep voltammetry (LSV) polarization curve of TPA_TPT_COF catalyst at all rotation speeds 625 to 4900 rpm in O_2 saturated 0.1 M KOH electrolyte solution
Fig. S20	Linear sweep voltammetry (LSV) polarization curve of TPT_TPB_COF and TPB_TPA_COF catalysts at all rotation speeds 625 to 4900 rpm in O_2 saturated 0.1 M KOH electrolyte solution and corresponding KL plots
Fig. S21	Linear sweep voltammetry (LSV) polarization curve of TPA_TPT_COF catalyst at 1600 rpm in O_2 saturated 0.1 M KOH electrolyte solution with ring and disk current
Fig. S22	Linear sweep voltammetry polarization curve before and after stability of TPA_TPT_COF catalyst
Fig. S23	Full survey of XPS analysis of TPA_TPT_COF catalyst and deconvoluted C1s and N1s spectra after stability measurement
Fig. S24	Methanol cross over durability (i-t) curve of TPA_TPT_COF in presence of 1 M methanol in O_2-saturated 0.1 M KOH solution and comparison with Pt/C catalyst
Fig. S25	CV analysis of TPA_TPT_COF electro catalyst with 1 M CH_3OH and without CH_3OH in O_2-saturated 0.1 M KOH electrolyte.
Fig. S26	CV analysis of Pt/C catalyst with 1 M CH_3OH and without CH_3OH in O_2-saturated 0.1 M KOH electrolyte.
Fig. S27	In-situ FT-IR curve for ORR study in presence of argon

Section-S3	Theoretical study
Fig. S28	Diagrammatic representation of molecular orbital interaction between C, N, and O_2 on catalyst surface
Fig. S29	1:1 complex of TPA_TPT_COF with dual binding sites interact with O_2, optimized at B3LYP/6-31** level of theory
Fig. S30	1:1 complex of TPT_TPB_COF with dual binding sites interact with O_2, optimized at B3LYP/6-31** level of theory.
Fig. S31	1:1 complex of TPB_TPA_COF with dual binding sites interact with O_2, optimized at B3LYP/6-31** level of theory
Fig. S32	1:1 complex of TPA_TPT_COF, TPT_TPB_COF and TPB_TPA_COF with dual binding sites interact with O_2, optimized at B3LYP/6-31** level of theory
Table T1	Atomistic coordinates for the AA-stacking mode of TPA_TPT_COF
Table T2	Atomistic coordinates for the AA-stacking mode of TPT_TPB_COF
Table T3	Atomistic coordinates for the AA-stacking mode of TPB_TPA_COF
Table T4	Elemental analysis of TPA_TPT_COF, TPT_TPB_COF, and TPB_TPA_COF catalysts obtained from XPS analysis
Table T5	All the synthesized catalysts performances on the basis of electrocatalytic parameters for ORR
Table T6	Comparison table with recently reported COF materials for ORR analysis in 0.1 M KOH solution
Table T7	The table giving the bond distances of interaction with binding site of COF with O_2 and wiberg bond index (WBI) indicating about bond strength with respect of each one.
Table T8	The table giving the bond distances of interaction with binding site of COF with O_2 and wiberg bond index (WBI) indicating about bond strength with respect of each one on another active sites

Section-1: Materials and experimental section

Materials: The whole experiment was utilized tris(4-formylphenyl) amine was purchased from sigma Aldrich, India. O-dichlorobenzene(o-DCB) acetic acid (AcOH), potassium hydroxide (KOH)were also supplied by Sigma Aldrich, India. Ethanol(EtOH) was purchased from Spectro-chem, India, used with no further purification. The water used in all the experiments is was purified through a Milipore system.

Synthesis of 1, 3, 5-tris (4-formylphenyl)-benzene (TFPB)

1, 3, 5-Tribromobenzene (500 mg, 1.59 mmol), Na2CO3 (1.68 g, 15.9 mmol) and (4-formylphenyl) boronic acid (953 mg, 6.35 mmol) were dissolved in toluene (30 mL), water (5 mL) and ethanol (10 mL). The solution was degassed four times, Pd(PPh3)4 (183.7 mg, 0.159 mmol) was added under an argon atmosphere and the mixture was degassed 4 times again. The resulting solution was then heated at 90 °C for 48h. The organic layer was then decanted from the solution. The aqueous layer was extracted two times using CH_2Cl_2 solution. The combined organic layer was washed with water and evaporated. The crude product was purified by chromatography on silica gel using n-hexane/ EtOAc (10%) as the eluent to give the title compound TFPB as an off-white solid (465 mg, 75% yield).[1]

[1] H NMR (CDCl3, 400 MHz, ppm): δ 10.11 (s, 3H,), 8.03 (d, 6H), 7.91 (s, 3H), 7.86 (d, 6H).

Synthesis of 2, 4, 6-tris(4-aminophenyl)-1, 3, 5-triazine (TAPT):

We have taken 4-Amino benzonitrile (2 gm) in a round bottom flask equipped with an ice bath and 1 ml triflic acid was added to this drop-wise. The above prepared solution was then stirred

overnight at room temperature. 225 ml of distilled water was added to dilute the solution and the solution was neutralized with 2 (M) NaOH solution. A deep yellow color precipitate was washed with water several times and dried under vacuum. (Yellow solid, 1.9 g, 95%). [2]

^{1}H NMR (DMSO-d6, 400 MHz, ppm): δ 8.35 (d, 6H), 6.70 (d, 6H), 5.92 (s, 6H).

Synthesis of TPA_TPT_COF material

A 1:1 mixture of tris(4-formylphenyl)amine and 1,3,5-tris(4-aminophenyl) triazine along with 1:1:0.13 mixture of o-dichlorobenzene (o-DCB), ethanol (EtOH) and acetic acid (AcOH) were combined in a Pyrex glass tube. The mixture was then sonicated until a homogeneous solid precipitate formed and then flash frozen at 77 K in a liquid nitrogen bath and degassed 3 times to reduce the internal pressure to 10^{-3} mbar. The tube was then sealed and heated in an oil bath at 125°C for 4 days. After continuous heating for 4 days, the tube was cooled, and the resulting light-yellow precipitate was filtered and washed several times with acetone. The resulting precipitate was then dried to a powder in an oven at 80°C. Finally, the product TPA_TPT_COF was obtained, with a yield of 76% as shown in reaction below.

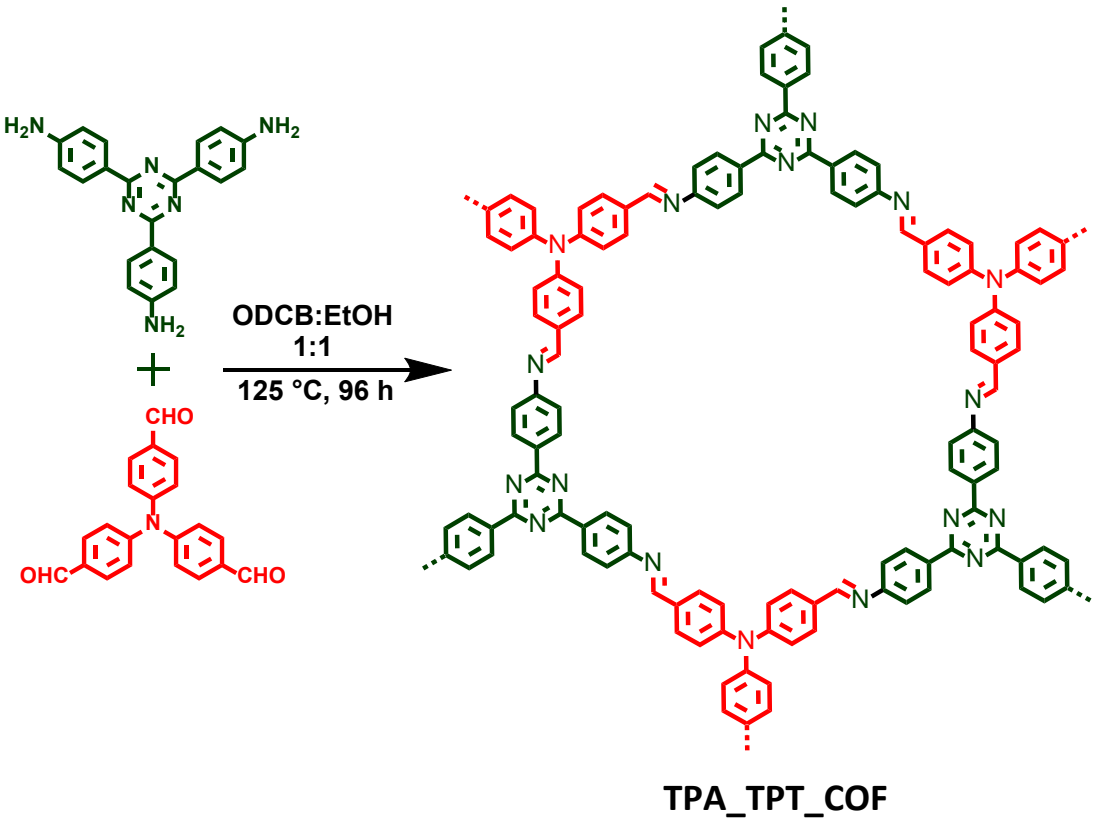

TPA_TPT_COF

Synthesis of TPT_TPB_COF

To synthesize the above TPT_TPB_COF, an 1:1 mixture of 1,3,5-Tris(4 formylphenyl)benzene and 1,3,5-Tris(4-aminophenyl) triazine were taken in a Pyrex glass tube along mixture of Ethanol, o-dichlorobenzene (o-DCB) and acetic acid(AcOH) aqueous solution in a ratio of 1:1:0.13 . This mixture then ultra-sonicated till solid precipitate formed and then flash frozen in liquid N_2 bath at 77K followed by degassed it three times so that the internal pressure was decreased to 10^{-3} mbar. Then this tube was sealed and heated in an oil bath at 120°C for 4 days. After 4 days of continuous heating the tube was cooled and the green yellow precipitate obtained was filtered and washed with acetone several times. Then the obtained precipitate was dried to powder in an oven at 80°C. Finally, the Product TPT_TPB_COF was obtained with a yield of 72% as shown in the reaction below:

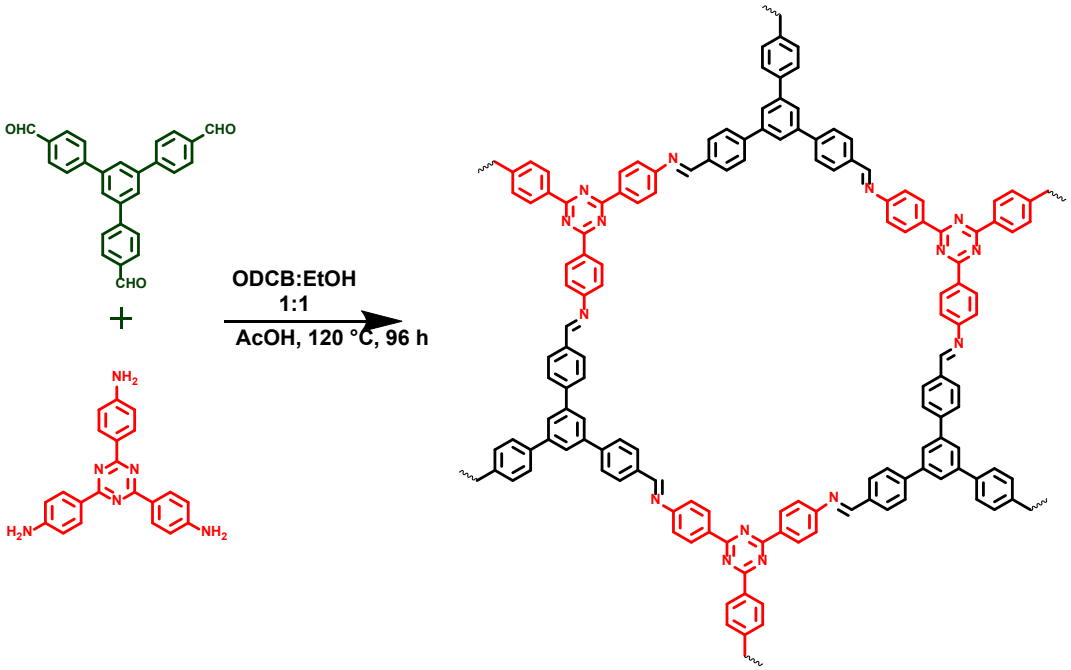

TPT_TPB_COF

Synthesis of TPB_TPA_COF

Tris(4-aminophenyl) amine and 1,3,5-Tris(4-formylphenyl) benzene were mixed with 1:1 ratio in a Pyrex glass tube along with 1:1:0.13 mixture of Ethanol, o-dichlorobenzene (o-DCB) and acetic acid(AcOH) aqueous solution. This mixture then ultra-sonicated till solid precipitate formed and then flash frozen in liquid N_2 bath at 77K followed by degassed it three times so that the internal pressure was decreased to 10^{-3} mbar. Then this tube was sealed and heated in an oil bath at 120°C for 4 days. After 4 days of continuous heating the tube was cooled and the brown orange precipitate obtained was filtered and washed with acetone several times. Then the obtained precipitate was dried to powder in an oven at 80°C. Finally, the Product TPB_TPA_COF was obtained with a yield of 70% as shown in the reaction below:

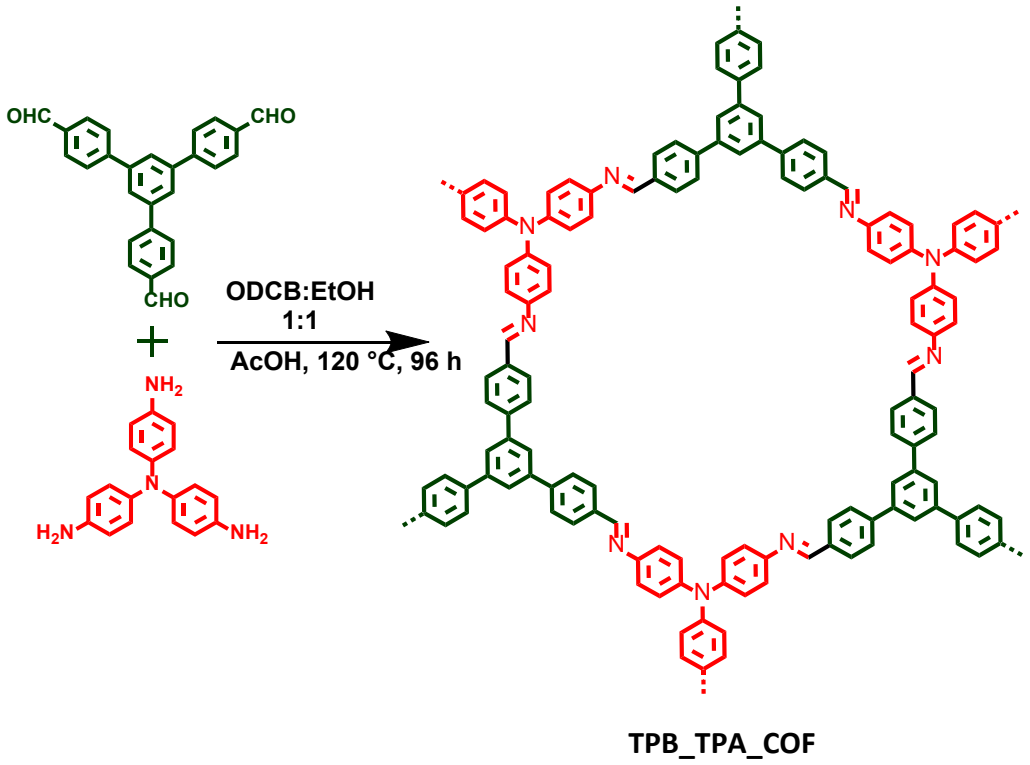

TPB_TPA_COF

Instrumentation.

To analyze the crystal structure of the samples, Powder X-ray diffraction (PXRD) analysis were carried out with Bruker D8 Advances instrument with Cu-Kα (λ = 1.5406 Å) radiation in the 2θ range from 10° to 70° with an acceleration voltage of 40 KV. The solid-state ^{13}C NMR spectroscopy analysis was measured using NMR600 instrument facility form Saif, IIT Bombay. To confirm structural analysis, JEOL NMR600 instrument was used. The high-resolution transmission electron microscope (HRTEM, JEM2100 instrument) was used to further characterize the detailed surface morphology. For surface area analysis, N_2 sorption analysis was carried out in an Anton Paar Quanta Tec Inc. iSorb HP1, gas adsorption analyzer at 77 K. COF sample was degassed at 150 ^oC for 3 h prior to the sorption measurement. To determine the pore size and to calculate the specific surface area of the samples, Non-local density functional theory (NLDFT) model and Brunauere-Emmette-Teller (BET) were used respectively. X-ray photoelectron spectroscopy (XPS) was performed to determine the bonding configuration and surface elemental composition using spectrometer (K-Alpha 1063) instruments in an ultrahigh vacuum chamber ($7X10^{-9}$ torr). All these spectra mentioned above of the synthesized and other control materials were measured under ambient condition & the condition is maintained throughout the experiment.

Electrode preparation:

To prepare the ink at first the synthesized material was taken 5 mg with homogeneous mixture of water and isopropyl alcohol (1:1) followed by ultra sonication for 30 minutes. Before dropcating the sample, Glassy Carbon (GC), Rotating Disk Electrode (RDE)/Rotating Ring Disk Electrode (RRDE) were cleaned with 1,0.3 and 0.05 μm alumina(Al_2O_3) powder thoroughly and washed them with deionized water through ultra sonication. Then the ink was dropcated and kept in overnight for vacuum drying. In another case Pt/C catalyst 20 wt %) was prepared on the same manner with the addition of Nafion (5%).The mass ration of Pt/C was optimized for the comparison with our synthesized catalyst. All these electrochemical reaction was carried out under room temperature.

Electrochemical Measurements

Electrochemical measurements such as Cyclic Voltammetry (CV) & Linear Sweep Voltammetry (LSV) were carried out with a Rotating Ring Disk Electrode (RRDE; GC area 0.196 cm^2, Pt ring area 0.041 cm^2). All these measurements were carried out in Autolab multichannel electrochemical workstation with a three electrode cell including Ag/AgCl (3M KCl) as a reference electrode, Pt as a counter electrode & RRDE as a working electrode. 0.1 M KOH was used as an electrolyte. To conduct these experiments, Ar or O_2 were purged for 30 minutes depending upon our requirements & the same condition was maintained throughout the experiment. Although all the experiments were carried out with Ag/AgCl as a reference electrode, the final potentials were converted into standard Reversible Hydrogen Electrode(RHE) by the following Nernst equation:

$$E_{RHE}\ (V) = E_{Ag/AgCl\ (3\ M\ KCl)}\ (in\ V) + (0.059 \times pH) + 0.210\ V \qquad \text{Eq. (1)}$$

The number of electron transfer (n) per O_2 participate in ORR can be determined by Koutecky Levich (K-L) equation

$$\frac{1}{J} = \frac{1}{J_L} + \frac{1}{J_K} = \frac{1}{B\omega^{\frac{1}{2}}} + \frac{1}{J_K} \qquad \text{Eq. (2)}$$

Where *j* is the measured current density, diffusion-limiting (J_L), kinetic current densities (J_K) and the number of electrons transferred (n) per O_2 molecule, ω is the angular velocity of the disk (ω = 2πN, N is the linear rotation speed), and B is the Levich slope.

B is given by:

$$B = 0.62nFC_0 D_0^{2/3} \vartheta^{-1/6} \qquad \text{Eq. (3)}$$

$$J_K = nFkC_0 \qquad \text{Eq. (4)}$$

Where J is the measured current density, J_L and J_K are the diffusion-limiting and kinetic current densities, C_0 is the bulk concentration of O_2 in the solution, F is the Faraday constant (F = 96485 C mol^{-1}), n is the overall number of electrons transferred in oxygen reduction reaction, ϑ is the kinematic viscosity of the electrolyte (1.09×10^{-2} cm^2 s^{-1}), and D_0 is the diffusion coefficient of O_2 in 0.1 M KOH (1.93×10^{-5} cm^2 s^{-1}).

The number of electron transferred & amount of H_2O_2 (%) were calculated by using these formulas;

$$\boldsymbol{n = 4 \times \frac{I_D}{I_D + \frac{I_R}{N}}} \qquad \text{Eq. (5)}$$

$$\boldsymbol{\%H_2O_2 = 200 \times \frac{\frac{I_R}{N}}{\frac{I_R}{N} + I_D}} \qquad \text{Eq. (6)}$$

where n is the number of electrons transferred (n) during the ORR process, Where I_D and I_R refers to disk current & ring current respectively; N is the current collection efficiency of Pt ring which is 0.249 in this case.

The electrochemical surface area(ECSA) of these three COF materials were calculated by using a three electrode system. To measure it cyclic voltammetry curve at different scan rates from 10 mV s^{-1} to 120 mV s^{-1} were taken in 0.1 M KOH electrolyte solution. The double layer capacitance (C_{dl})of all the materials were measured through CV curves in a non-faradaic region with various scan rates (5, 10, 20, 40, 60, 80, 100, 120 mV s^{-1}) by the following equation given below.

$$\mathbf{ECSA} = \frac{\boldsymbol{C_{dl}}}{\boldsymbol{C_s}} \qquad Eq.(7)$$

Where C_s is the specific capacitance

Section-2: Physical and electrochemical characterization

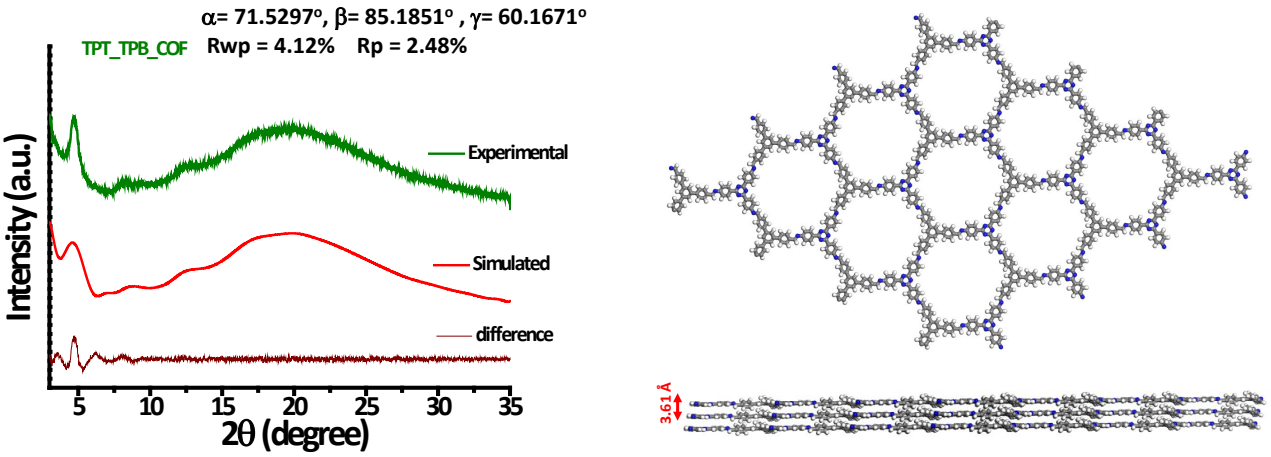

Fig. S1. (a) PXRD patterns of TPT_TPB_COF: experimental (green), Pawley refined (red), and the differences between the Pawley refined and experimental patterns (brown). (b) Perspective view (upper side) and side view (lower side) of TPT_TPB_COF in AA stacking ball-and-stick model (H atoms are omitted for clarity)

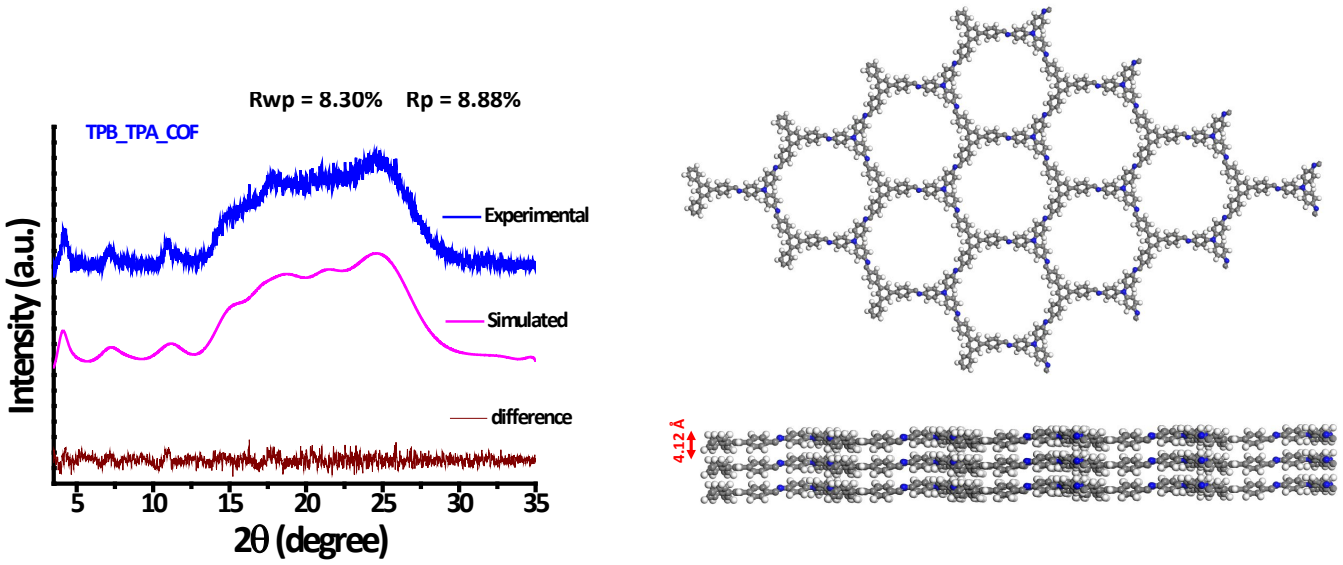

Fig. S2. (a) PXRD patterns of TPB_TPA_COF: experimental (blue), Pawley refined (magenta), and the differences between the Pawley refined and experimental patterns (brown). (b) Perspective view (upper side) and side view (lower side) of TPB_TPA_COF in AA stacking ball-and-stick model (H atoms are omitted for clarity)

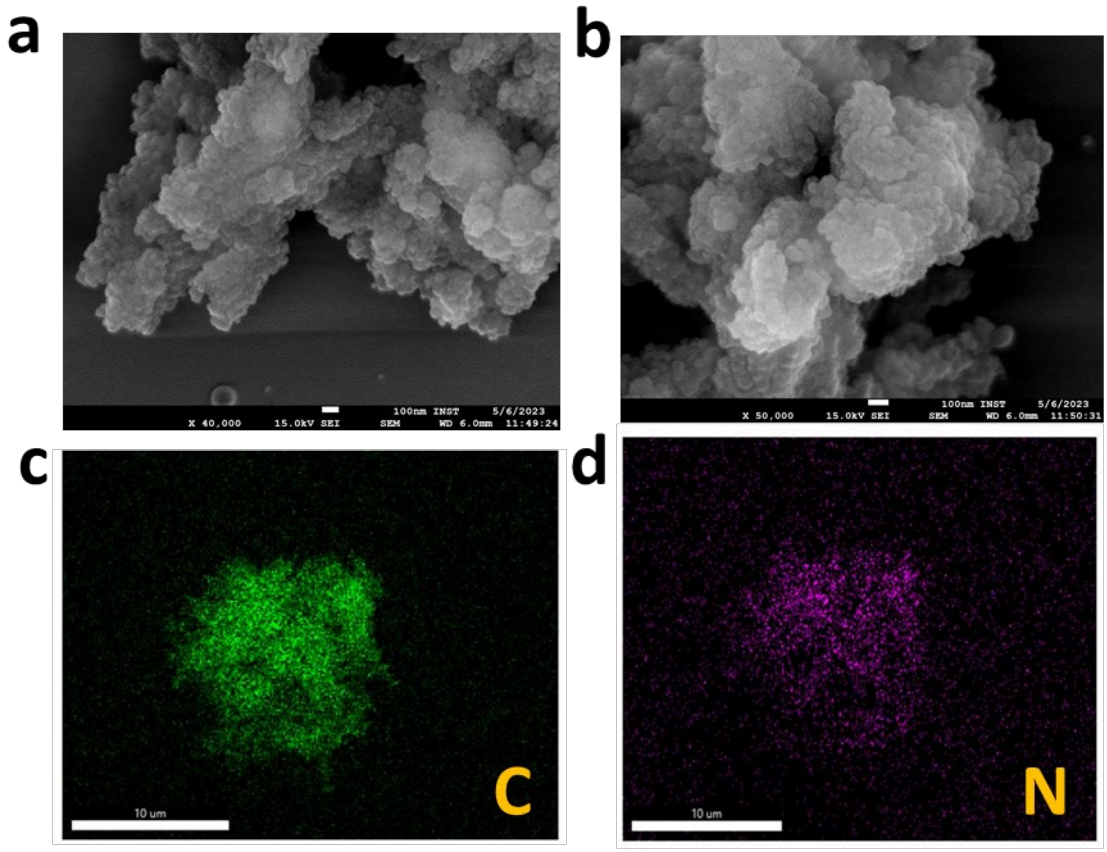

Fig. S3. (a-b) FESEM image of TPA_TPT_COF material and (c-d) elemental mapping of TPA_TPT_COF electrocatalyst.

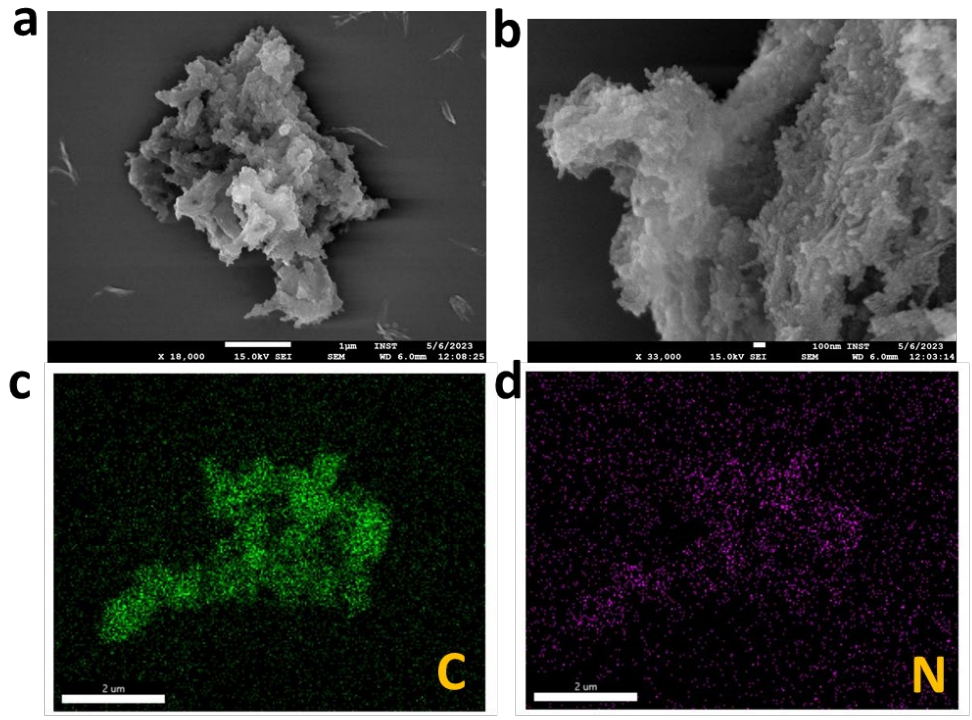

Fig. S4. (a-b) FESEM images of TPT_TPB_COF catalyst

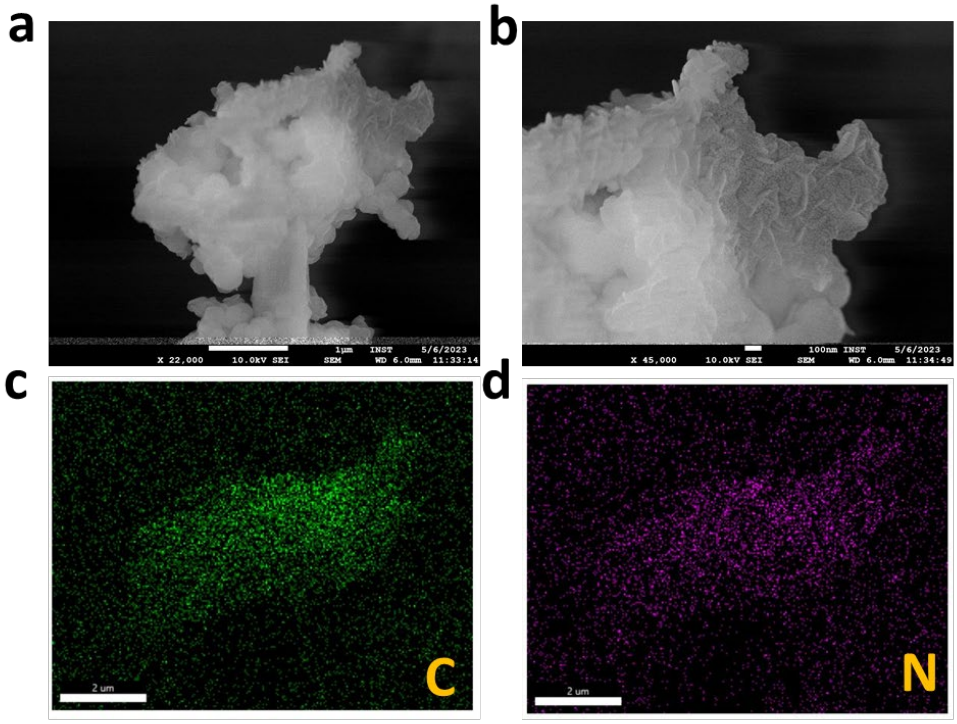

Fig. S5. (a-b) FESEM images of TPB_TPA_COF catalyst.

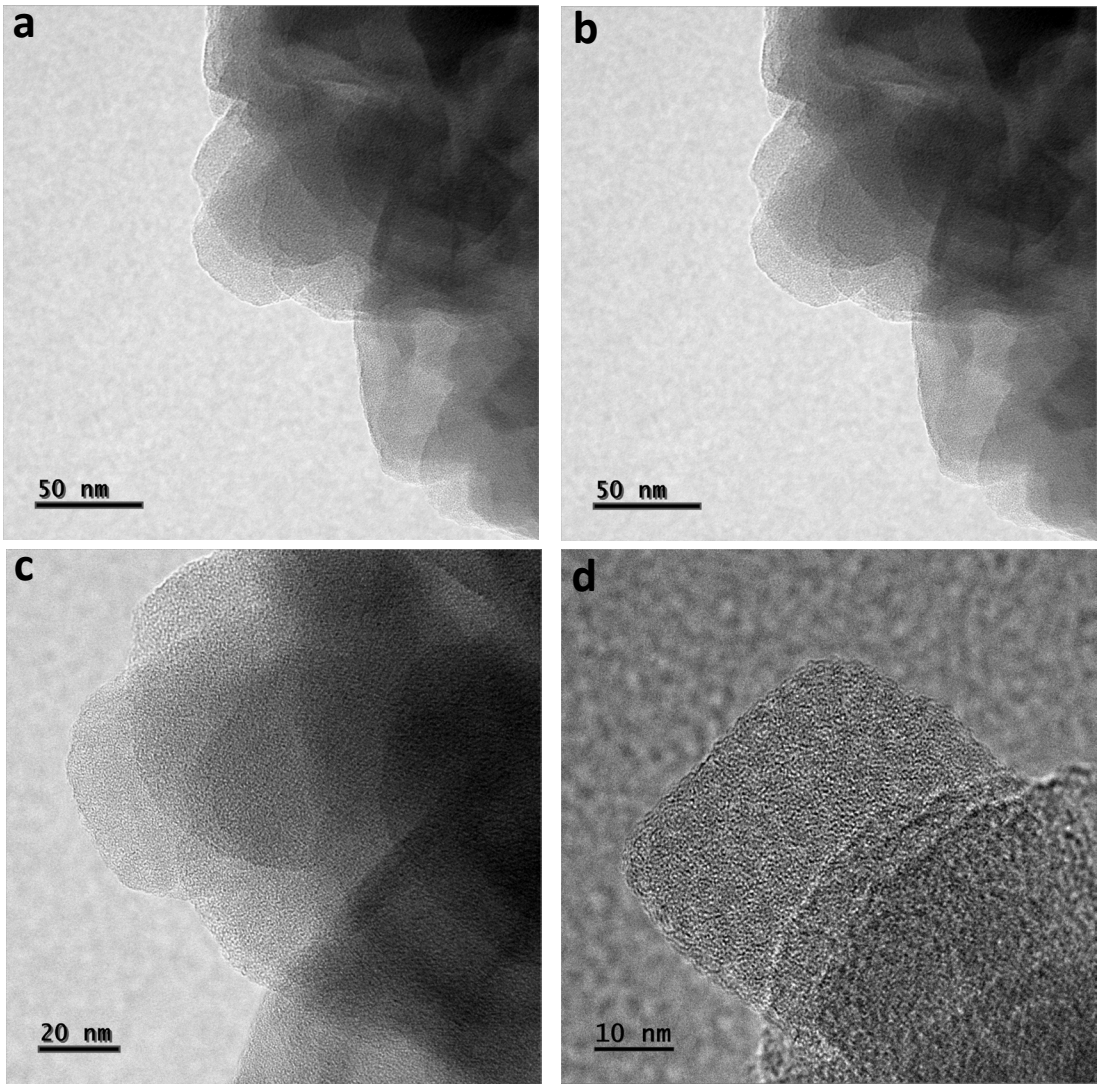

Fig. S6. (a-d) HRTEM images of TPA_TPT_COF catalyst

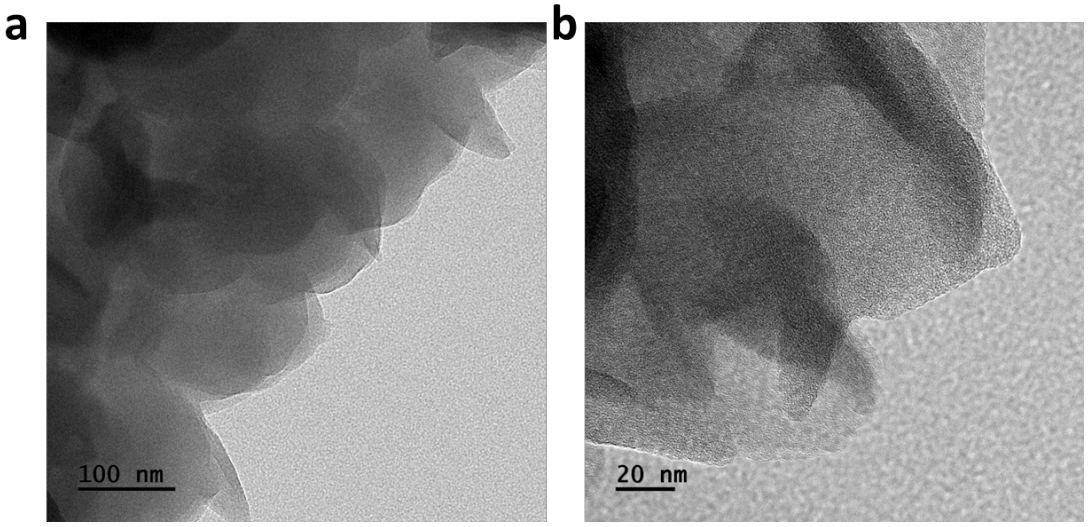

Fig. S7. (a-b) HRTEM images of TPT_TPB_COF catalyst

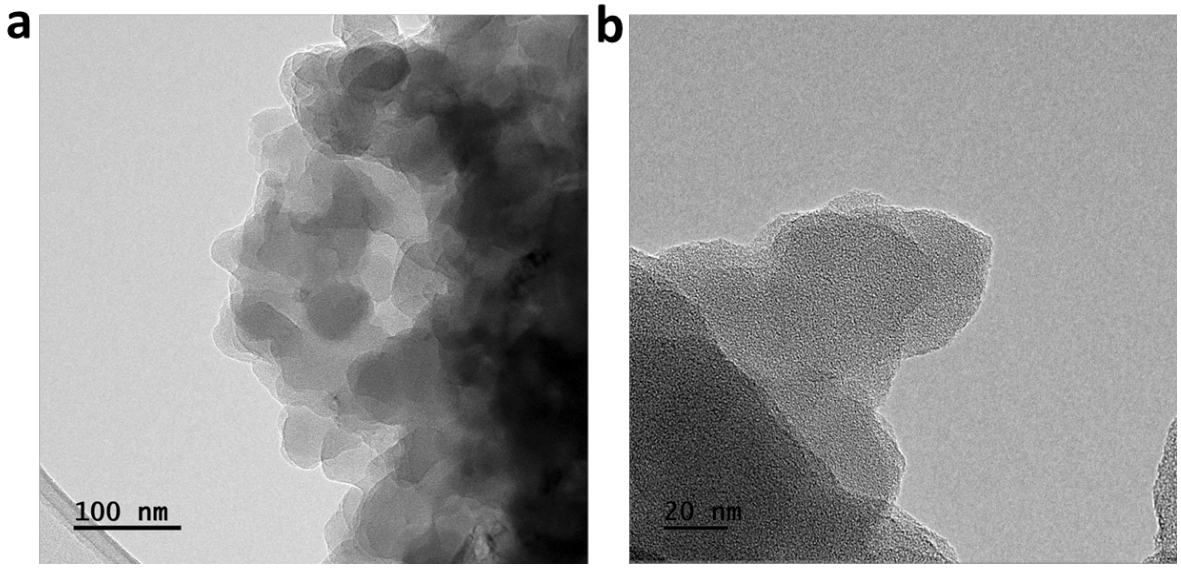

Fig. S8. (a-b) HRTEM images of TPB_TPA_COF catalyst

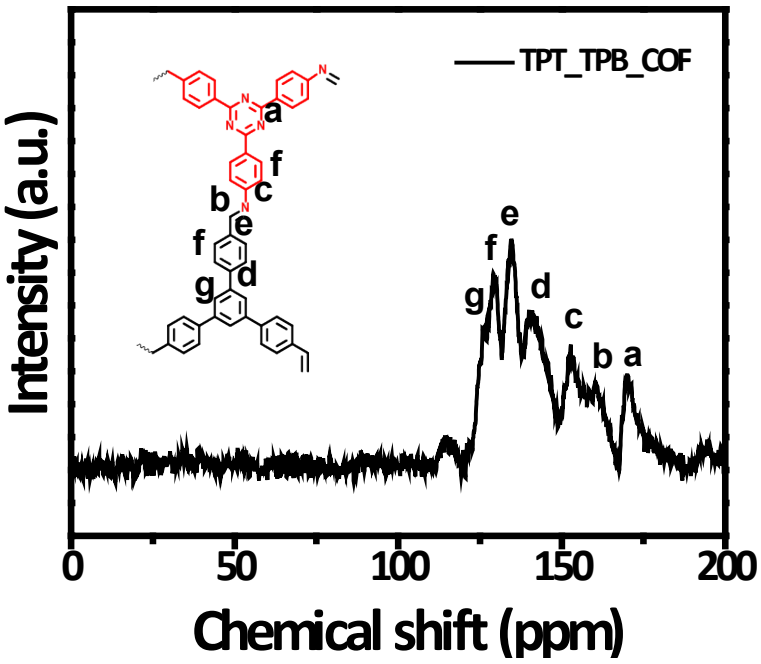

Fig. S9. Solid state ^{13}C NMR of TPT_TPB_COF materials

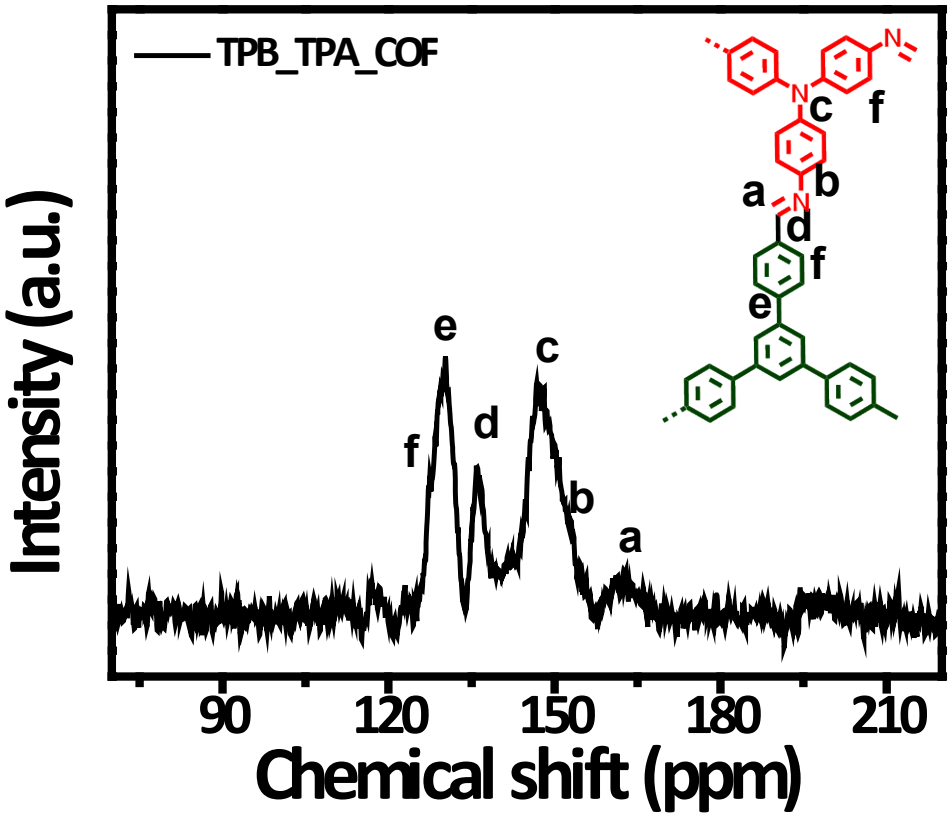

Fig. S10. Solid state ^{13}C NMR of TPB_TPA_COF material.

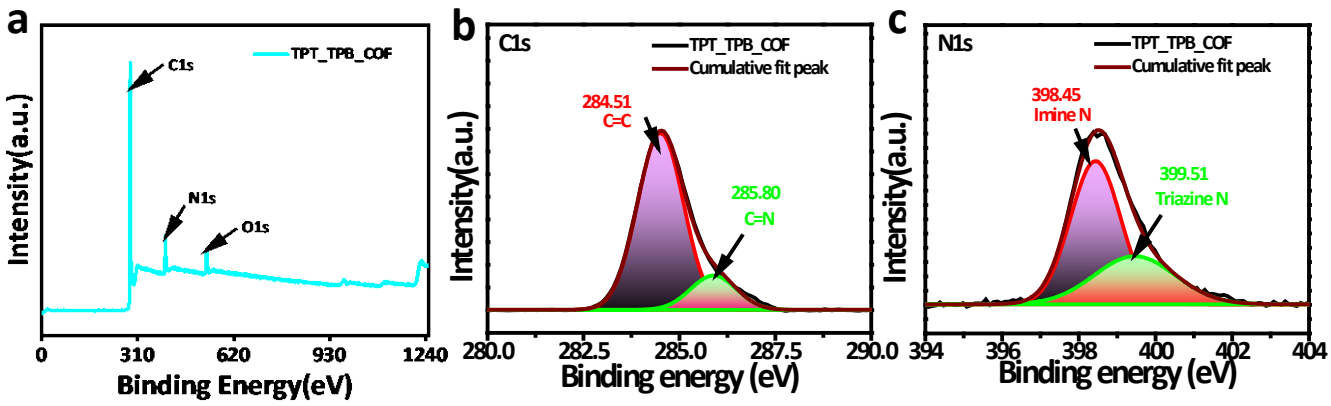

Fig. S11. (a) Full survey of XPS analysis of TPT_TPB_COF catalyst (b) High-resolution deconvoluted C1s XPS spectra. (c) High-resolution deconvoluted N1s XPS spectra.

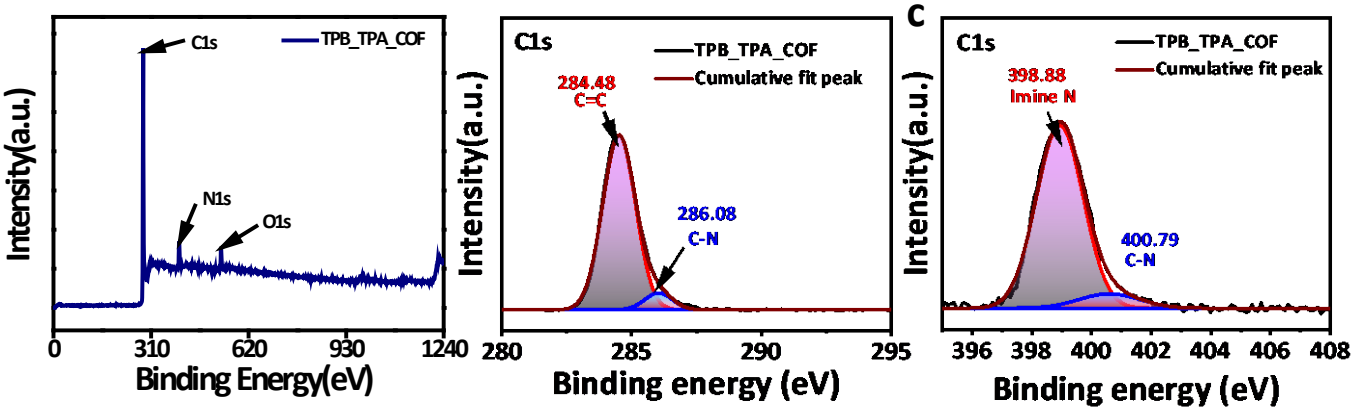

Fig. S12. (a) Full survey of XPS analysis of TPB_TPA_COF catalyst (b) High-resolution deconvoluted C1s XPS spectra. (c) High-resolution deconvoluted N1s XPS spectra.

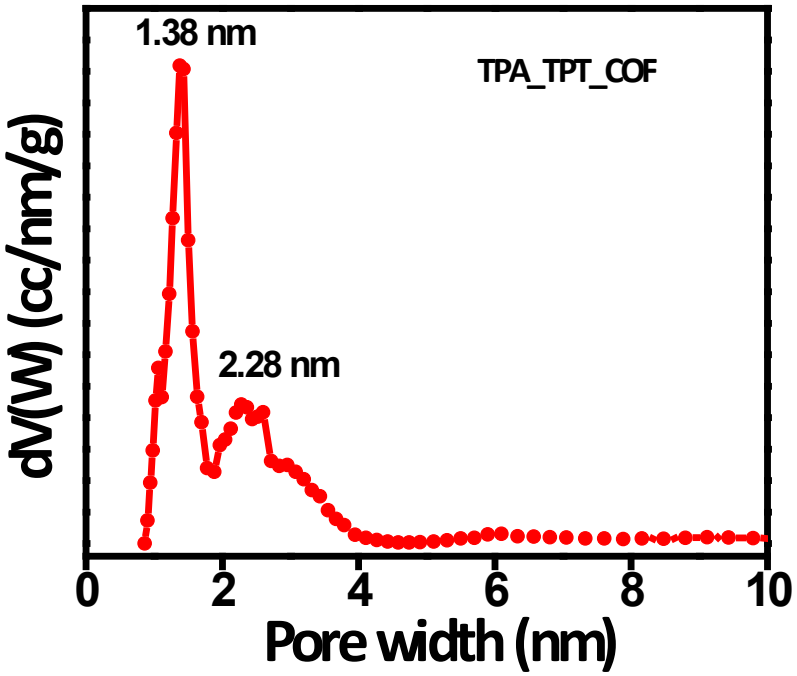

Fig. S13. The pore size distribution (PSD) for the TPA_TPT_COF material

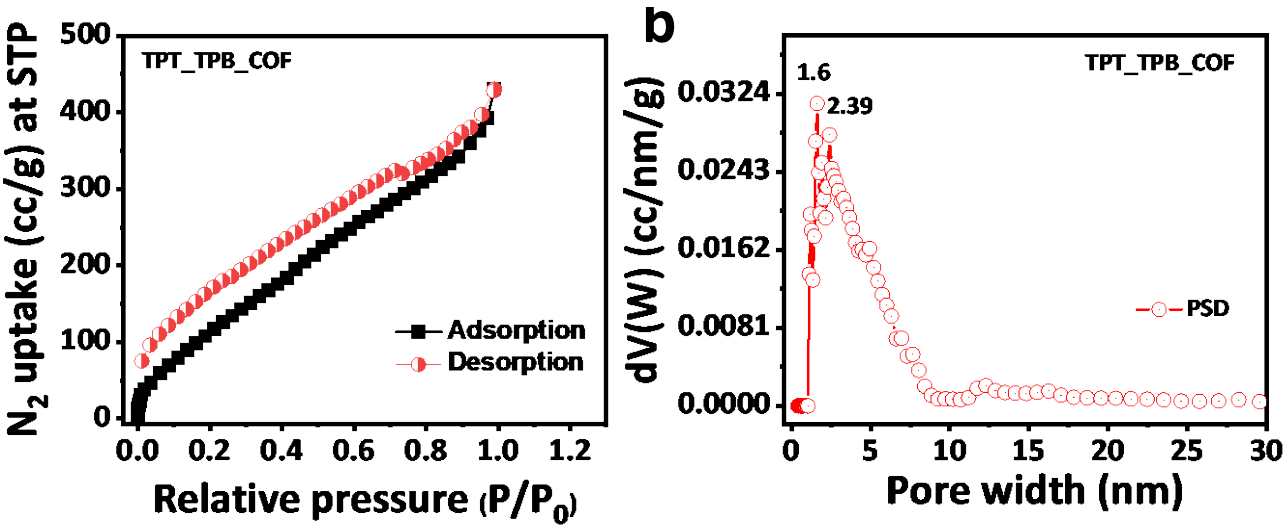

Fig. S14. (a) BET adsorption/desorption isotherm and (b) pore size distribution (PSD) for the TPT_TPB_COF material

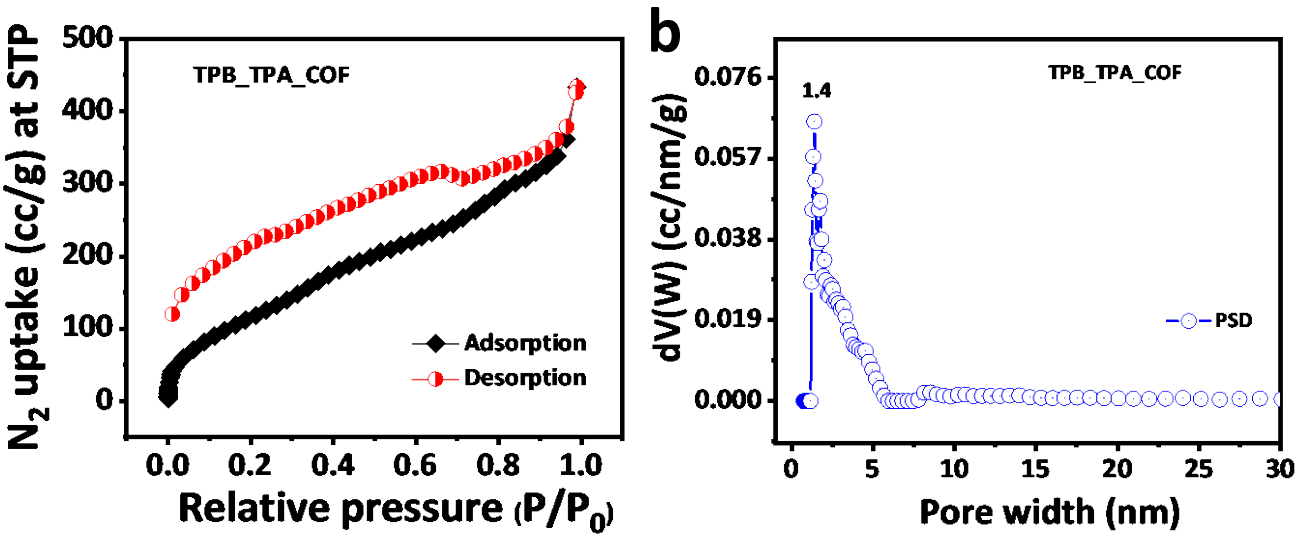

Fig. S15. (a) BET adsorption/desorption isotherm and (b) pore size distribution (PSD) for the TPB_TPA_COF material

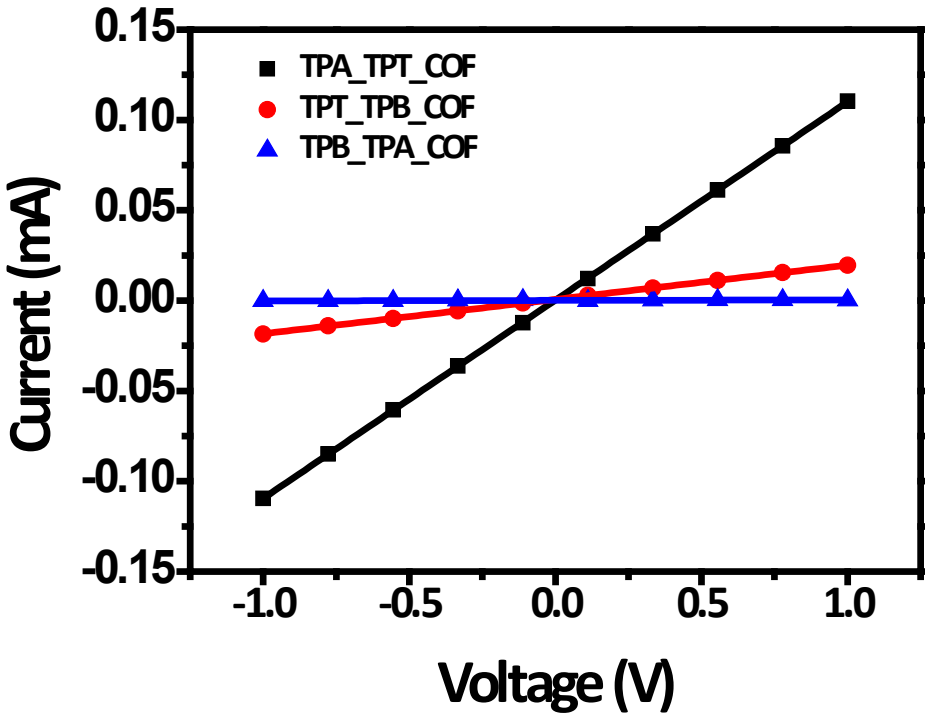

Fig. S16. Electrical sheet resistance measurement (i–v) curve of TPA_TPT_COF, TPT_TPB_COF and TPB_TPA_COF catalysts

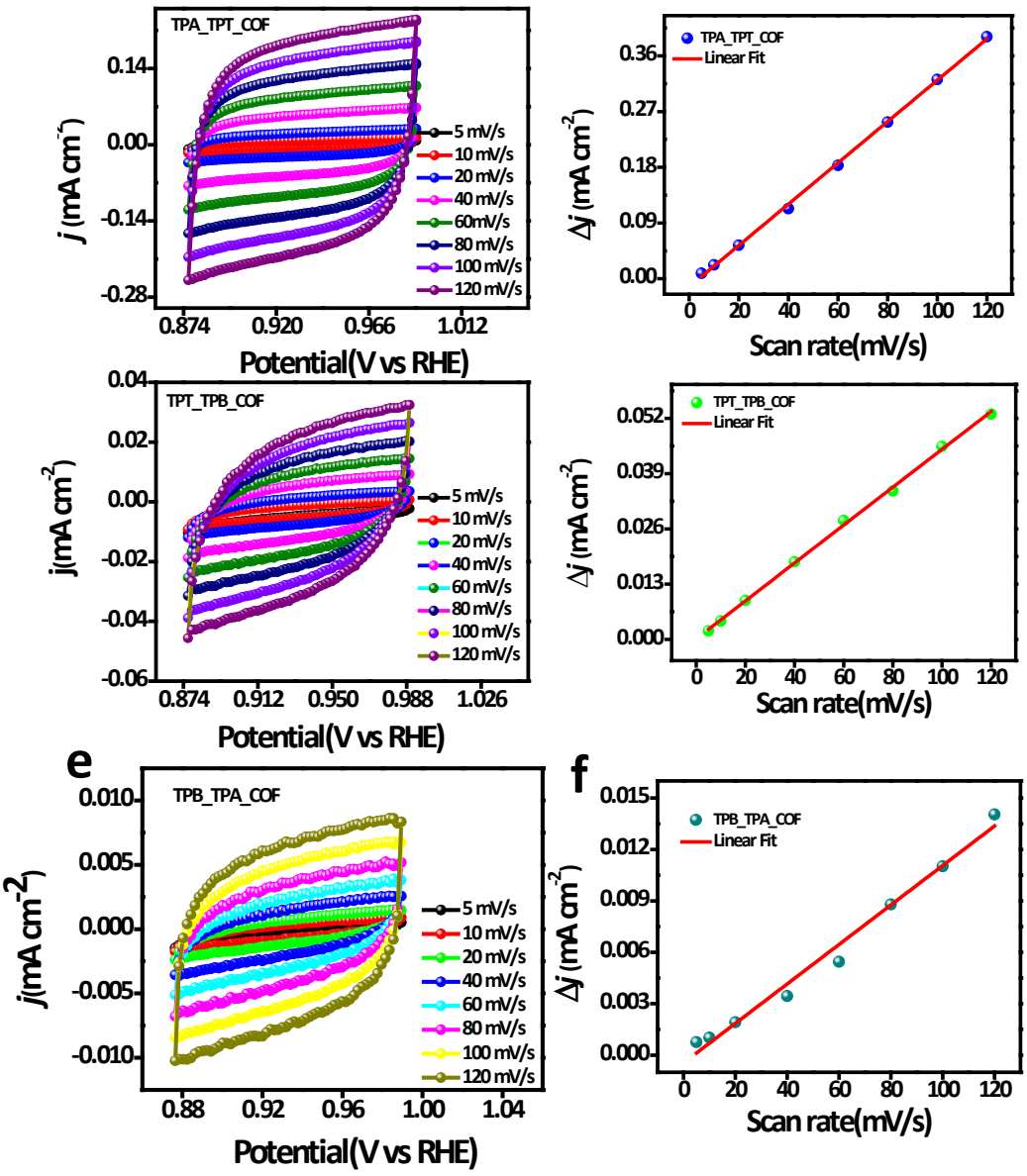

Fig. S17. Electrochemical active surface area analysis (a) CV curves of TPA_TPT_COF catalyst at different scan rate (b) Linear fitting of capacitive currents of the TPA_TPT_COF catalyst vs scan rate (c) CV curves of TPT_TPB_COF catalyst at different scan rate (d) Linear fitting of capacitive currents of the TPT_TPB_COF catalyst vs scan rate (e) CV curves of TPB_TPA_COF catalyst at different scan rate (f) Linear fitting of capacitive currents of the TPB_TPA_COF catalyst vs scan rate.

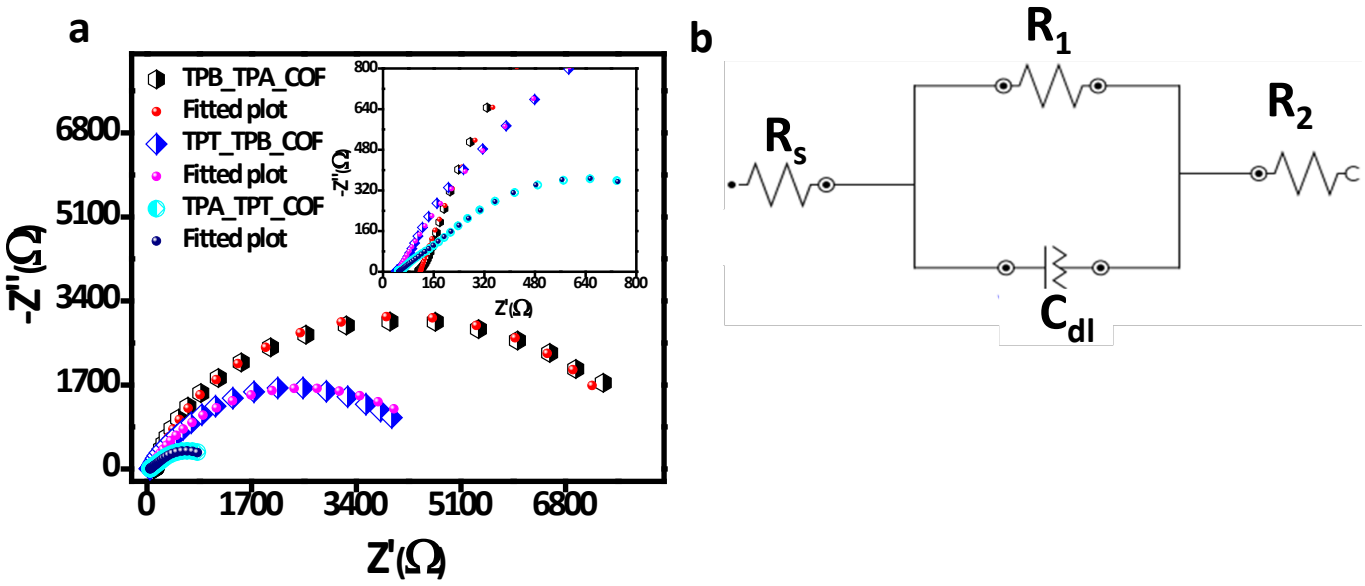

Fig. S18. (a) Electrochemical impedance spectroscopy (EIS) spectra of TPA_TPT_COF, TPT_TPB_COF, TPB_TPA_COF (inset; zoomed data of all the COF materials) and (b) equivalent fitted circuit of materials.

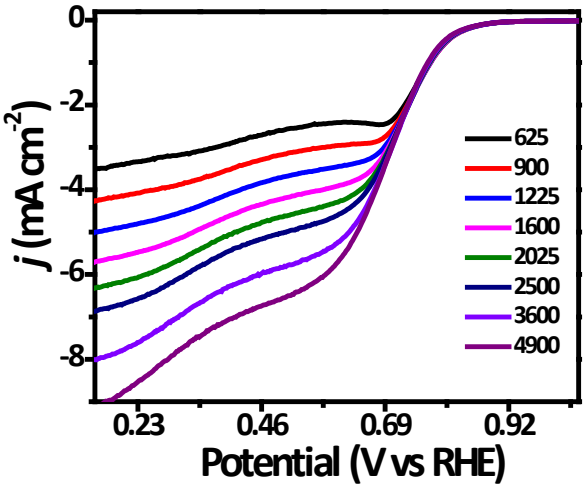

Fig. S19. (a) Linear sweep voltammetry (LSV) polarization curve of TPA_TPT_COF catalyst at all rotation speeds 625 to 4900 rpm in O_2 saturated 0.1 M KOH electrolyte solution.

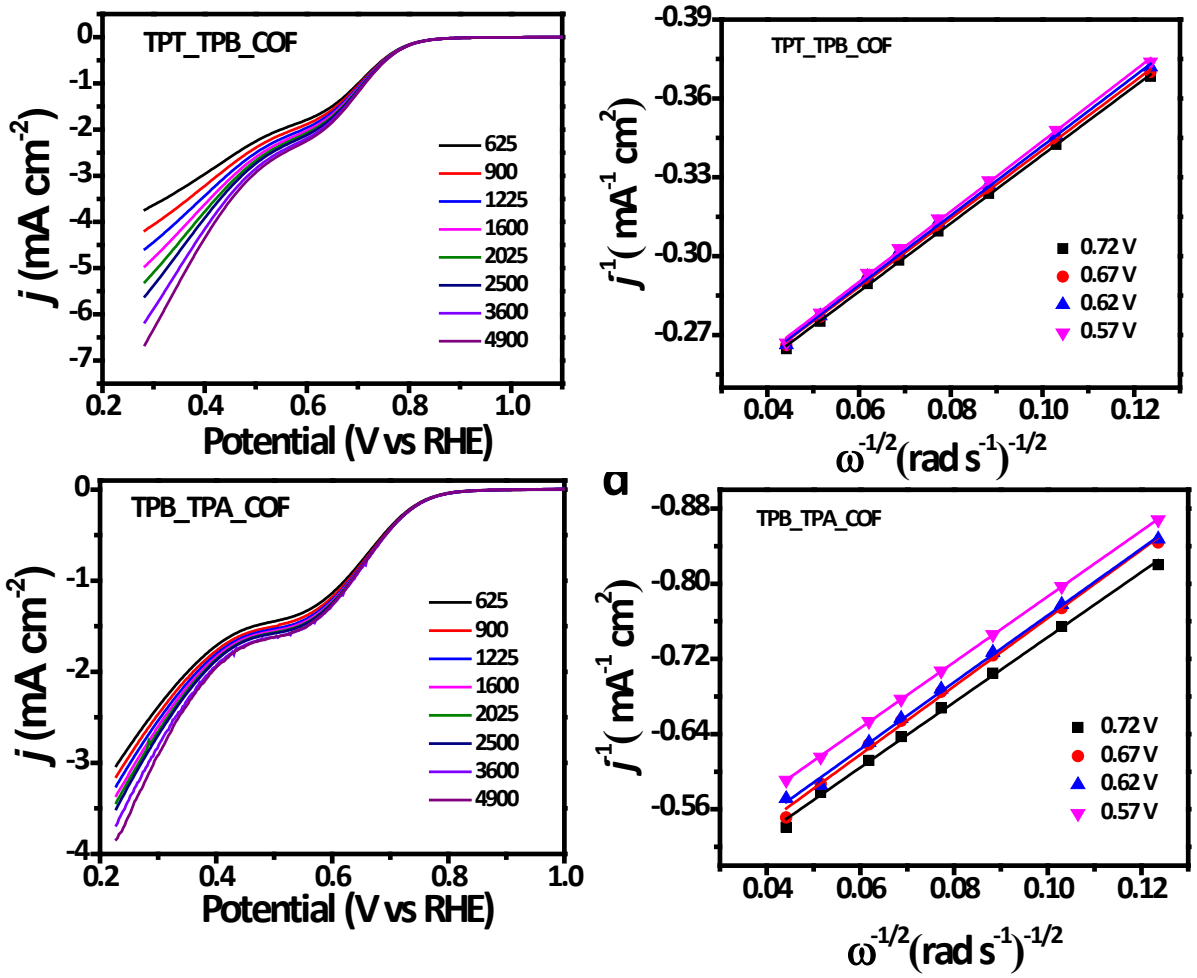

Fig. S20. (a) Linear sweep voltammetry (LSV) polarization curve of TPT_TPB_COF catalyst at all rotation speeds 625 to 4900 rpm in O_2 saturated 0.1 M KOH electrolyte solution. (b) KL plots of TPT_TPB_COF at different potentials. (c) Linear sweep voltammetry (LSV) polarization curve of TPB_TPA_COF catalyst at all rotation speeds 625 to 4900 rpm in O_2 saturated 0.1 M KOH electrolyte solution. (d) KL plots of TPB_TPA_COF at different potentials.

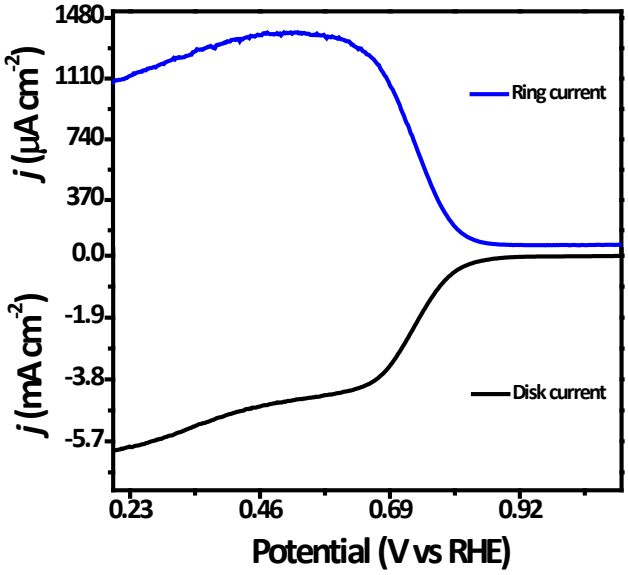

Fig. S21. Linear sweep voltammetry (LSV) polarization curve of TPA_TPT_COF catalyst at 1600 rpm in O_2 saturated 0.1 M KOH electrolyte solution with ring and disk current.

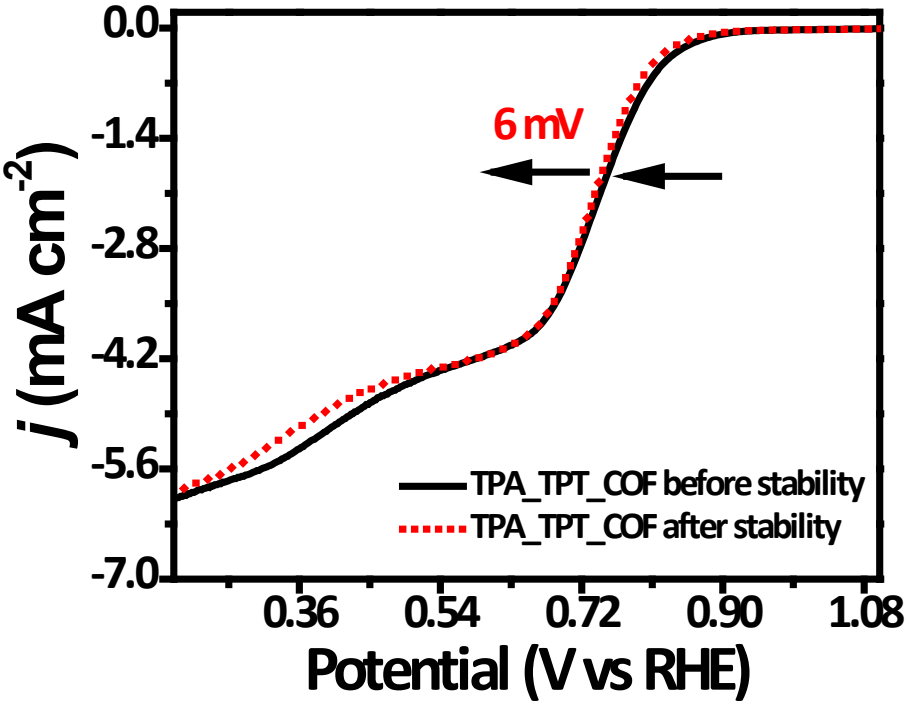

Fig. S22. Linear sweep voltammetry polarization curve before and after stability of TPA_TPT_COF electro catalyst.

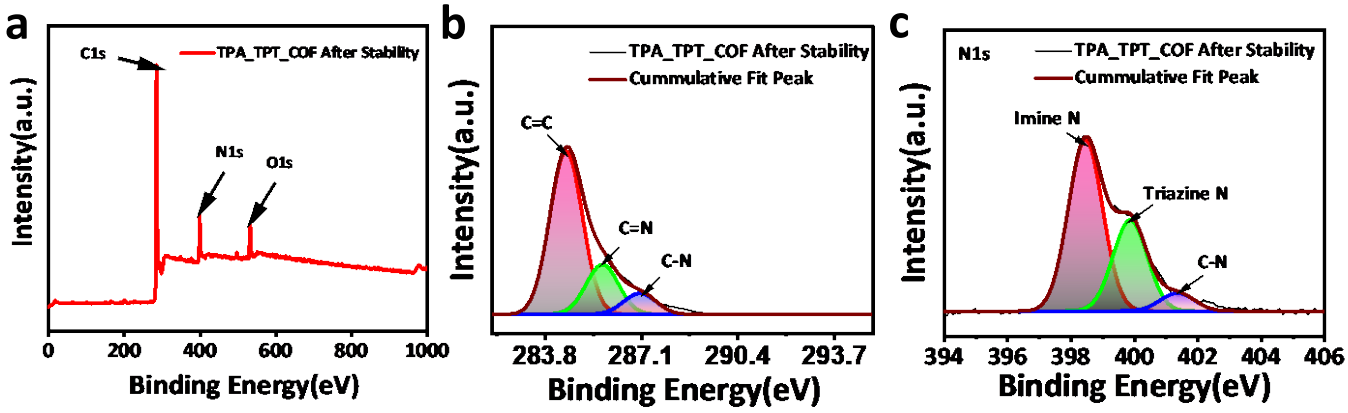

Fig. S23. (a) Full survey of XPS analysis of TPA_TPT_COF catalyst after stability measurement (b) High-resolution deconvoluted C1s XPS spectra. (c) N1s deconvoluted spectra after stability measurent.

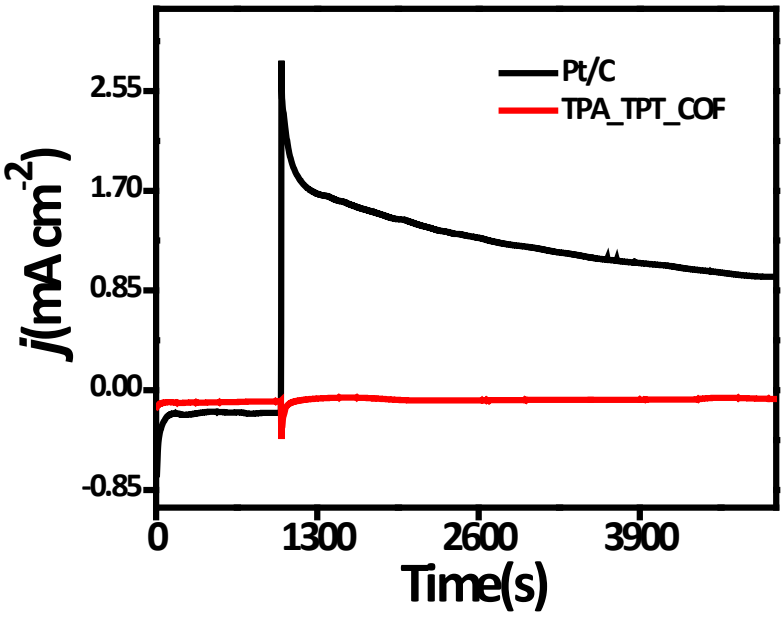

Fig. S24. Methanol cross over durability (i-t) curve of TPA_TPT_COF in presence of 1 M methanol in O_2-saturated 0.1 M KOH solution and comparison with Pt/C catalyst.

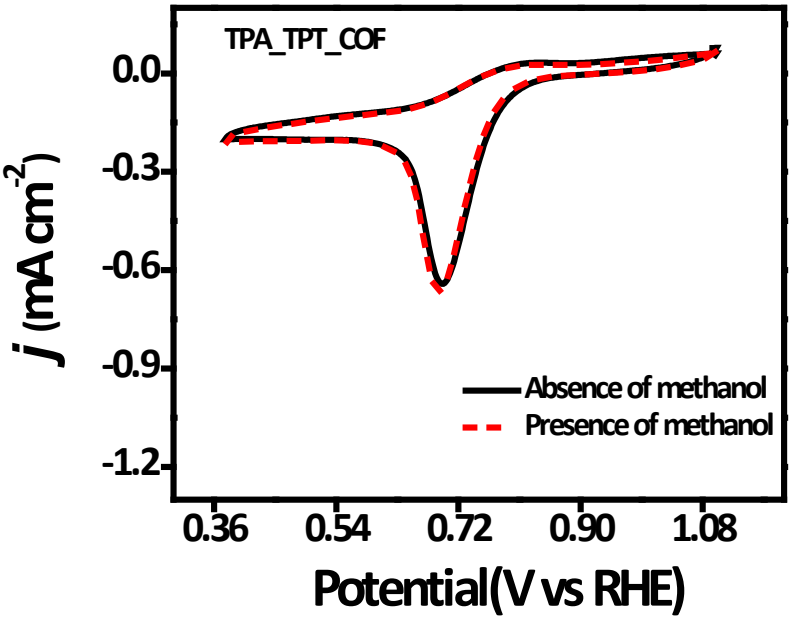

Fig. S25. CV analysis of TPA_TPT_COF electro catalyst with 1 M CH_3OH and without CH_3OH in O_2-saturated 0.1 M KOH electrolyte.

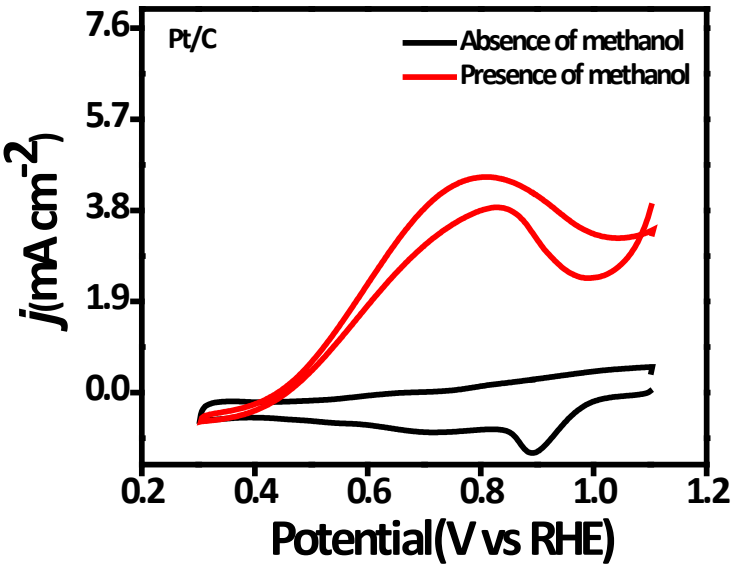

Fig. S26. CV analysis of Pt/C catalyst with 1 M CH_3OH and without CH_3OH in O_2-saturated 0.1 M KOH electrolyte.

The in-situ electrochemical attenuated total reflection infrared (ATR-IR) spectroscopy of the TPA_TPT_COF catalyst:

The in-situ ATR-IR spectroscopic study for the ORR intermediate detection have been performed in Argon and O_2 saturated alkaline media The chronoamperometry study at different potentials (1.0, 0.90, 0.80, 0.70, 0.60, 0.50, and 0.40 V vs RHE) in Argon and O_2-saturated alkaline electrolytes was performed. The Insitu IR spectra was recorded and intermediate products detected as explained in the main manuscript file. The peak intensity enhancement clearly indicates the formation of the water as a final product in the ORR catalysis.

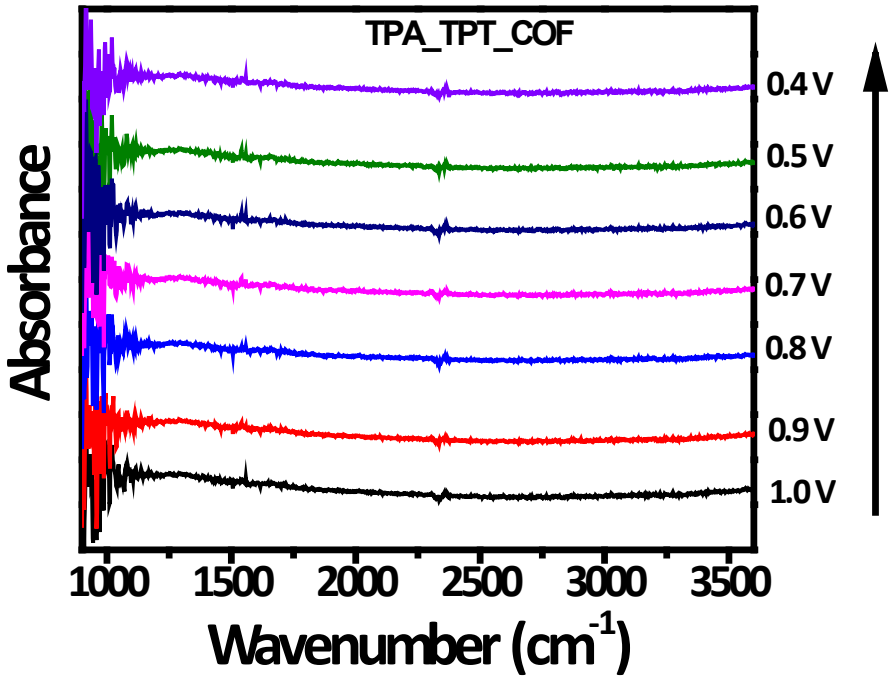

Fig. S27. In-situ ATR-IR curve for TPA_TPT_COF in argon-saturated alkaline media for ORR study

Section-3 Theoretical Study

Computational Methodology: In this investigation, we have used Gaussian16 RevB.01 ref Quantum chemical software for all DFT calculations. The Grimme's dispersion-corrected B3LYP functional (B3LYP-D3) was employed for geometry optimization.[3,4] Geometry optimization and computation of imaginary frequencies were performed species. The basis set 6-31G** basis set used for C, H, N, and O, in the calculations.[3–5] Frequency calculations were conducted to identify minima on the potential-energy surface (PES) and determine free energy correction energy. Optimized geometries were visualized using Chemcraft 1.6 (ChemCraft software, version 1.6). Gaussian16 software was used for NBO (Natural Bond Orbital and WBI (Wiberg Bond Index) analyses using DFT methods at B3LYP/Def2TZVP level of theory including Grimme's Dispersion GD3.[6] NBO analysis provided detailed insights into bonding orbitals and WBI analysis offered bond index values indicating bond nature.

The zero-point vibrational energy (ZPVE) corrected complexation energy was calculated according to the following equation.

$$\Delta E_{Comp}^{ZPVE} = \Delta E_{Comp}^{ZPVE} - E_{COF}^{ZPVE} - E_{O2}^{ZPVE} \qquad Eq.8$$

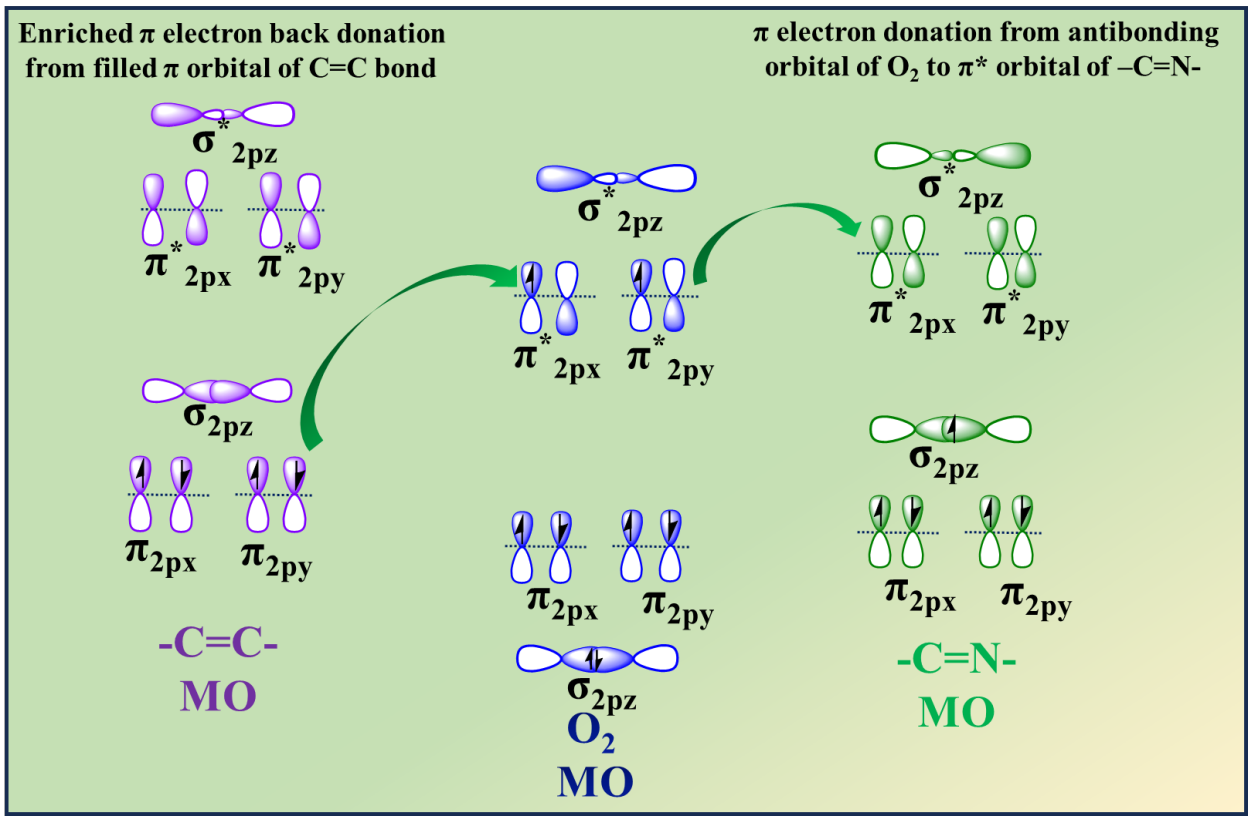

Fig. S28. Diagrammatic representation of molecular orbital interaction between C, N, and O_2 on TPA_TPT_COF catalyst surface.

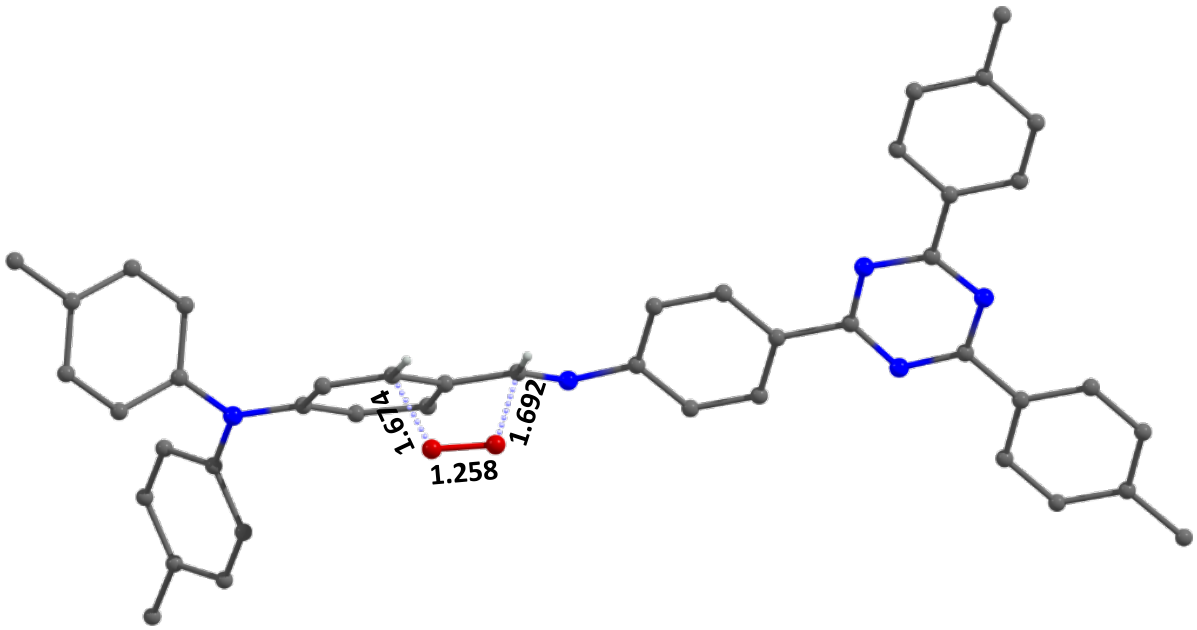

Fig. S29. 1:1 complex of TPA_TPT_COF with dual binding sites interact with O_2, optimized at B3LYP/6-31** level of theory. The bond length of the adsorbed O_2 is mentioned in Å for each complex, showing that O_2 bond length in these complexes has increased compared to that of the pure O_2 [Hydrogens are omitted for clarity; colour code: red- oxygen, blue- nitrogen, dark grey- carbon atoms]

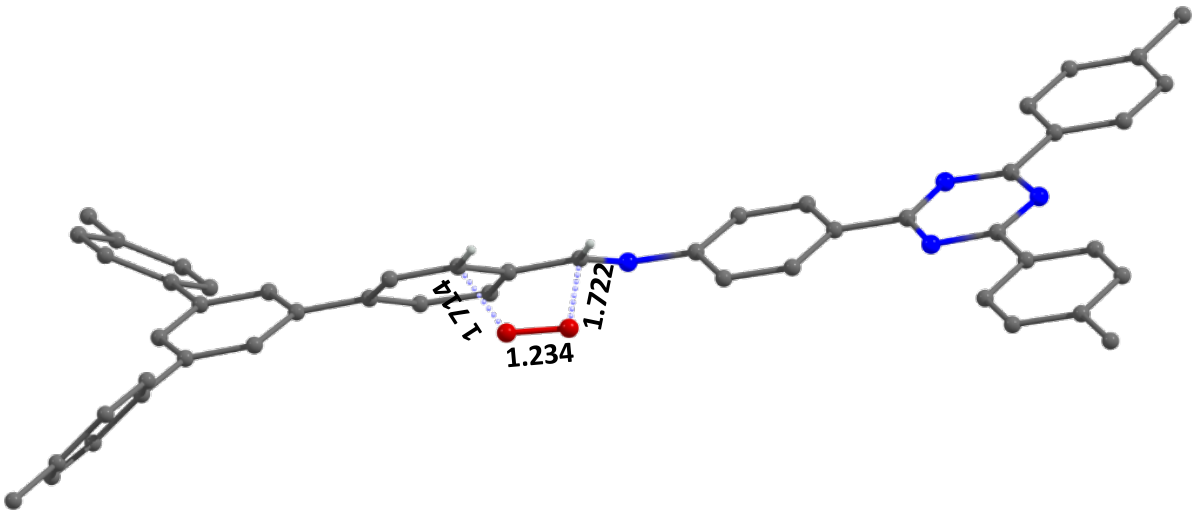

Fig. S30. 1:1 complex of TPT_TPB_COF with dual binding sites interact with O_2, optimized at B3LYP/6-31** level of theory. The bond length of the adsorbed O_2 is mentioned in Å for each complex, showing that O_2 bond length in these complexes has increased compared to that of the pure O_2 [Hydrogens are omitted for clarity; colour code: red- oxygen, blue- nitrogen, dark grey- carbon atoms]

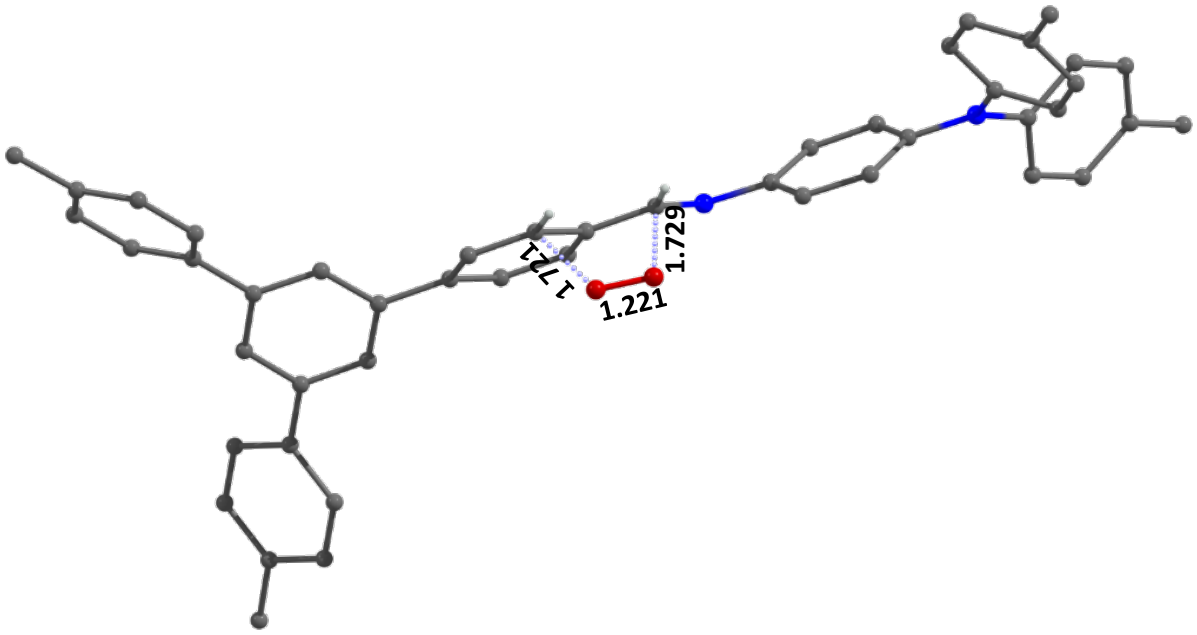

Fig. S31. 1:1 complex of TPB_TPA_COF with dual binding sites interact with O_2, optimized at B3LYP/6-31** level of theory. The bond length of the adsorbed O_2 is mentioned in Å for each complex, showing that O_2 bond length in these complexes has increased compared to that of the pure O_2 [Hydrogens are omitted for clarity; colour code: red- oxygen, blue- nitrogen, dark grey- carbon atoms]

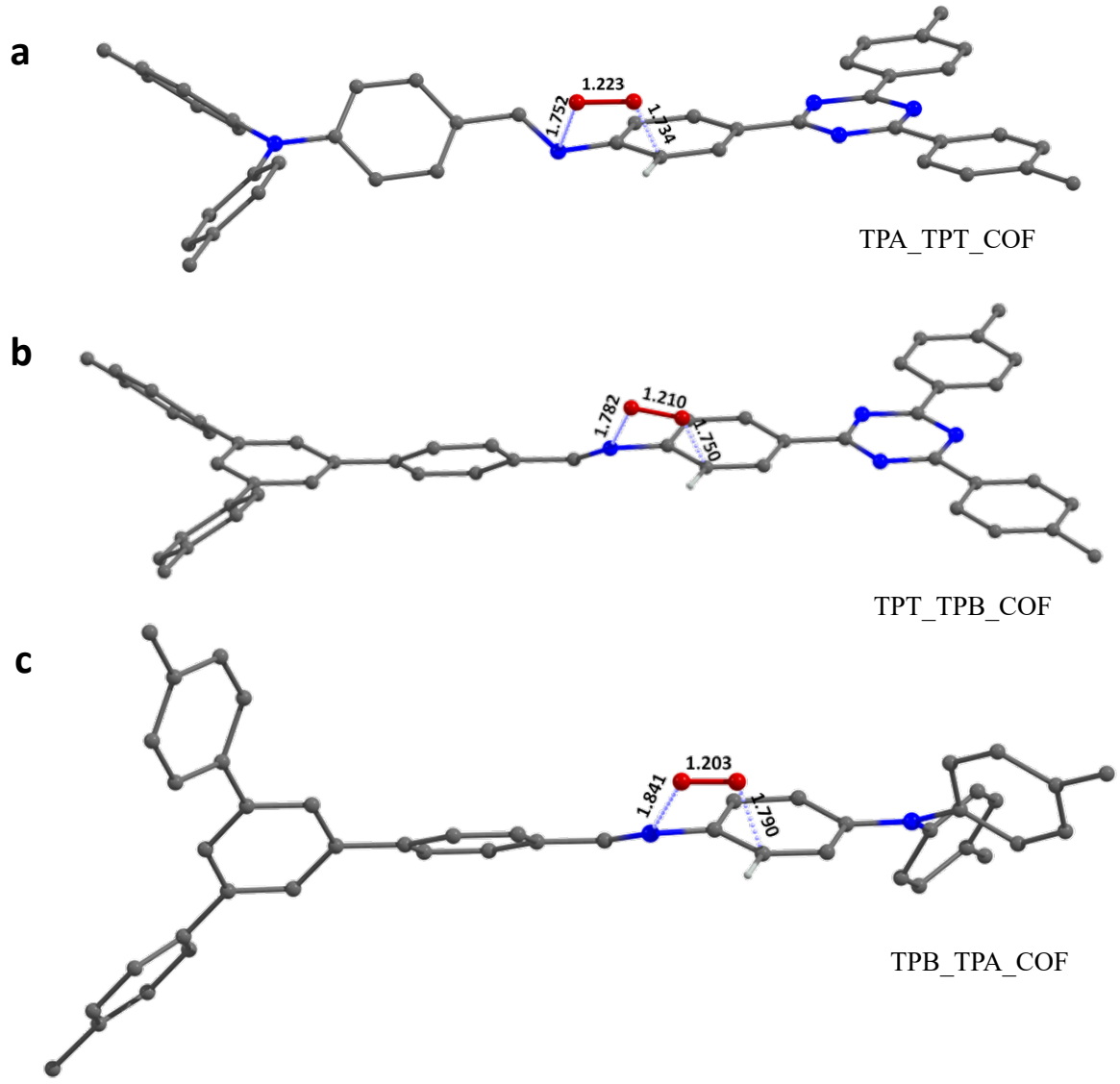

Fig. S32. The 1:1 complex of (a) TPA_TPT_COF (b) TPT_TPB_COF, and (c) TPB_TPA_COF with dual binding sites interact with O_2, optimized at B3LYP/6-31** level of theory. The bond length of the adsorbed O_2 is mentioned in Å for each complex, showing that O_2 bond length in these complexes has increased compared to that of the pure O_2 [Hydrogens are omitted for clarity; colour code: red- oxygen, blue- nitrogen, dark grey- carbon atoms]

Table 1. Atomistic coordinates for the AA-stacking mode of TPA_TPT_COF (space group P3, a = b = 23.6074 Å, c = 3.9443 Å, α = β = 90° and γ = 120°, Rwp = 6.17 % and Rp = 4.24 %)

Atom	x/a	y/b	z/c
C1	0.62367	1.36161	0.8888
C2	0.64259	1.42224	1.0449
C3	0.60184	1.44934	1.04488
C4	0.5402	1.41627	0.88997
C5	0.52046	1.35599	0.73466
C6	0.56159	1.32932	0.73323
C7	0.49602	1.44361	0.88736
N8	0.51302	1.4993	1.03237
C9	0.47456	1.53095	1.04974
C10	0.50608	1.59729	1.13609
C11	0.47129	1.63075	1.15217
C12	0.40375	1.59803	1.08633
C13	0.37173	1.53097	1.0082
C14	0.40667	1.49765	0.99015
C15	0.36708	1.63374	1.09489
N16	0.39953	1.70017	1.09459
H17	0.68952	1.44991	1.16232
H18	0.61869	1.49614	1.16723
H19	0.47306	1.32937	0.6131
H20	0.54366	1.2826	0.61544
H21	0.44989	1.41691	0.75498

H22	0.55811	1.62336	1.18757
H23	0.49733	1.68222	1.21689
H24	0.31968	1.50424	0.95767
H25	0.38001	1.44597	0.93332
N26	0.66667	1.33333	0.88852

Table 2. Atomistic coordinates for the AA-stacking mode of TPT_TPB_COF (space group P1 Triclinic, a = 26.0351 b = 26.0975 Å, c = 3.6091 Å, α = 71.5297 β = 85.1851° and γ = 60.1671°, Rwp = 4.12 % and Rp = 2.48 %)

Atom	**x/a**	**y/b**	**z/c**
C1	0.8541	0.2505	0.54998
C2	0.89037	0.27498	0.58311
C3	0.8658	0.337	0.57748
C4	0.80361	0.37436	0.54624
C5	0.76645	0.35144	0.50592
C6	0.79211	0.2899	0.50246
C7	0.70078	0.39141	0.47423
C8	0.67312	0.45515	0.25671
C9	0.60354	0.40367	0.6378
C10	0.61139	0.49277	0.23209
C11	0.57606	0.4674	0.42192
C12	0.90494	0.36271	0.60371
C13	0.88622	0.42625	0.41594
C14	0.96191	0.32395	0.80828
C15	0.92301	0.45028	0.43554
C16	0.88078	0.18374	0.57299
C17	0.8499	0.15108	0.72639
C18	0.93799	0.15124	0.45429
C19	0.87511	0.08838	0.75624

C20	0.96345	0.08831	0.48956
C21	0.93216	0.05637	0.64027
N22	1.00086	0.49473	0.5338
N23	0.01075	0.95925	0.57593
C24	0.04004	0.8954	0.58502
C25	0.00904	0.86342	0.60105
C26	0.10156	0.86481	0.56272
C27	0.03958	0.8017	0.60123
C28	0.13218	0.80305	0.56374
C29	0.13364	0.7057	0.57536
C30	0.22347	0.6154	0.56676
C31	0.13234	0.61634	0.56493
N32	0.10327	0.67602	0.57066
N33	0.19373	0.67516	0.5715
N34	0.19244	0.58632	0.56441
C35	0.09888	0.58446	0.55643
C36	0.12913	0.52087	0.59012
C37	0.0364	0.6173	0.51144
C38	0.09765	0.49065	0.584
C39	0.00498	0.58705	0.50386
C40	0.03509	0.5235	0.54495
C41	0.28896	0.58237	0.56103
C42	0.3204	0.51849	0.60247
C43	0.32077	0.6142	0.51482

C44	0.38214	0.48729	0.59685
C45	0.38254	0.58297	0.50676
C46	0.41364	0.51918	0.54409
N47	0.47711	0.48469	0.54452
C48	0.51101	0.50803	0.39493
C49	0.66522	0.36614	0.66431
C50	0.10148	0.77082	0.58147
H51	0.93801	0.24555	0.61472
H52	0.78383	0.42092	0.56531
H53	0.76342	0.27323	0.45459
H54	0.69913	0.4758	0.10112
H55	0.57749	0.38287	0.79044
H56	0.59116	0.5417	0.06224
H57	0.84367	0.45741	0.24488
C58	0.97981	0.41116	0.63832
H59	0.90728	0.49928	0.28673
H60	0.8068	0.1732	0.83448
H61	0.96308	0.17433	0.32659
H62	0.85029	0.06458	0.87603
H63	1.00735	0.06499	0.3934
C64	0.95763	-0.00977	0.67321
H65	-0.03869	0.88583	0.60599
H66	0.12596	0.88897	0.54634
H67	0.01447	0.77842	0.61312

H68	0.17982	0.78082	0.54741
H69	0.17724	0.49433	0.62069
H70	0.01166	0.66642	0.48127
H71	0.12259	0.4421	0.60203
H72	-0.04313	0.61313	0.46873
H73	0.29742	0.49241	0.64076
H74	0.29801	0.66327	0.48558
H75	0.40557	0.43805	0.63024
H76	0.40563	0.60863	0.47936
H77	0.49204	0.55733	0.23923
H78	0.68516	0.31753	0.84017
C79	0.99893	0.34788	0.82282
C80	1.01951	0.43532	0.66462
H81	0.9779	0.27521	0.96458
H82	1.04236	0.31694	0.98411
H83	1.0637	0.40259	0.81091
H84	0.9312	0.96846	0.78646

Table 3. Atomistic coordinates for the AA-stacking mode of TPB_TPA_COF (space group P3 Trigonal, a = b = 23.6781 Å, c = 4.1252 Å, α = β = 90° and γ = 120°, Rwp = 8.30 % and Rp = 8.88 %)

Atom	x/a	y/b	z/c
C1	0.62917	1.36707	0.88575
C2	0.6525	1.42723	1.04596
C3	0.61637	1.45915	1.05214
C4	0.55545	1.43156	0.89732
C5	0.53192	1.37215	0.73584
C6	0.5682	1.34038	0.72994
C7	0.51633	1.46221	0.90079
N8	0.53261	1.51622	1.05182
C9	0.49085	1.54582	1.04886
C10	0.51103	1.60383	1.21993
C11	0.47245	1.63317	1.22341
C12	0.41306	1.60527	1.05242
C13	0.39319	1.54703	0.87966
C14	0.43152	1.51741	0.87923
C15	0.37214	1.63677	1.05369
N16	0.40129	1.70506	1.0538
H17	0.69909	1.45027	1.16427
H18	0.63607	1.5052	1.17894
H19	0.48508	1.35022	0.6149

H20	0.54768	1.29421	0.60837
H22	0.55638	1.62605	1.35468
H23	0.48859	1.67699	1.36593
H24	0.34872	1.52497	0.73838
H25	0.41514	1.47285	0.7425
H	1.26523	1.71912	1.05355
N26	0.66667	1.33333	0.8834

Table T4. Elemental analysis of TPA_TPT_COF, TPT_TPB_COF, and TPB_TPA_COF catalysts obtained from XPS analysis.

S No.	**Elements**	**TPA_TPT_COF Catalyst**		**TPA_TPT_COF Catalyst after stability**	**TPT_TPB_COF Catalyst**	**TPB_TPA_COF Catalyst**
		Binding Energy (eV)	**Atomic (%)**	**Atomic (%)**	**Atomic (%)**	**Atomic (%)**
1.	Carbon (C)	285.25	86.67	87.38	90.18	92.88
2.	Nitrogen (N)	399.23	13.33	12.62	9.82	7.12

Table T5. All the synthesized catalysts performances on the basis of electrocatalytic parameters for ORR

S. No.	Catalyst	Onset potential E_{onset} (V)	Half-wave potential $E_{1/2}$ (V)	Limiting current density J_L (mA cm^{-2})	Tafel slope (mV dec^{-1})
1	TPA_TPT_COF	0.93	0.75	5.9	75
2	TPT_TPB_COF	0.85	0.72	5.1	89
5	TPB_TPA_COF	0.83	0.70	3.35	99
6	Pt/C	0.998	0.85	5.7	76

Table T6. Comparison table with recently reported COF materials for ORR analysis in 0.1 M KOH solution

S. No.	Catalyst	Onset potential E_{onset} (V)	Half-wave potential $E_{1/2}$ (V)	Limiting current density J_L (mA cm^{-2})	Ref
1	**TPA_TPT_COF**	**0.93**	**0.75**		**This work**
2	**TPT_TPB_COF**	**0.85**	**0.72**		**This work**
3	**TPB_TPA_COF**	**0.83**	**0.70**		**This work**
4	Pt-COF_{800}	1.00 V	0.88	6.79	[7]
5	TRIPTA COF	0.77	0.68	3.1	[8]
6	H-Tp-COF Co-Tp-COF Ni-Tp-COF Mn-Tp-COF	0.71 V 0.81 V 0.72 V 0.75 V	0.65 V 0.73 V 0.66 V 0.680 V	 4.8 5.0	[9]
7	1.JUC-606 2.JUC-605	0.79 V -	0.70 V 0.65 V	3.77 2.42	[10]
8	1.JUC-527	0.77 V	0.63 V		[11]

	2.JUC-528	0.82 V	0.70 V		
9	COP-PSO3-Co-rGO	0.88 V	0.72 V		[12]
10	TZA-COF	0.86 V	0.76 V		[13]
11	NDI-COF	0.85 V	0.70 V		[14]
12	Trz COP		0.73 V	5.2	[15]
13	**1**. TAB-HKH-COF **2**.TAB-HKH-COF-CNT	0.73 V 0.86 V	0.69 V 0.79 V	0.8 5.5	[16]
14	JUC-608	0.84 V	0.72 V	-	[17]
15	DAPT-TFP-COF	0.79	0.69	-	[18]
16	DAF-COF	0.89	0.74		[19]
17	TAPTt	0.85 V	0.74 V		[20]
18	COF-JLU-82 COF-JLU-23	0.98 V 0.99 V	0.68 V 0.66 V		[21]
19	CTFs	0.75 V	0.60 V		[22]
20	Azo-COF	0.88 V	0.68 V		[23]

Table T7: The table giving the bond distances of interaction with binding site of COF with O_2 and wiberg bond index (WBI) indicating about bond strength with respect of each one.

Species	Bond Distances			Wiberg Bond Index (WBI)		
	O_1-O_2	C_N-O_1	C_C-O_2	O_1-O_2	C_N-O_1	C_C-O_2
TPA_TPT_COF	1.285	1.692	1.674	1.23	0.38	0.47
TPT_TPB_COF	1.234	1.714	1.722	1.30	0.33	0.39
TPB_TPA_COF	1.221	1.721	1.729	1.34	0.29	0.35

Table T8: The table giving the bond distances of interaction with binding site of COF with O_2 and wiberg bond index (WBI) indicating about bond strength with respect of each one.

Species	Bond Distances			Wiberg Bond Index (WBI)		
	O_1-O_2	N-O_1	C-O_2	O_1-O_2	N-O_1	C-O_2
TPT-TPA_COF	1.223	1.752	1.734	1.28	0.31	0.38
TPT_TPB_COF	1.210	1.782	1.750	1.34	0.27	0.30
TPB_TPA_COF	1.203	1.841	1.790	1.39	0.22	0.27

References

1 B. C. Patra, S. K. Das, A. Ghosh, A. K. Raj, P. Moitra, M. Addicoat, S. Mitra, A. Bhaumik, S. Bhattacharya and A. Pradhan, *J. Mater. Chem. A*, 2018, **6**, 16655–16663.

2 S. Kanti Das, S. Mishra, K. Manna, U. Kayal, S. Mahapatra, K. Das Saha, S. Dalapati, G. P. Das, A. A. Mostafa and A. Bhaumik, *Chem. Commun.*, 2018, **54**, 11475–11478.

3 J. Antony and S. Grimme, *Phys. Chem. Chem. Phys.*, 2006, **8**, 5287–5293.

4 A. D. Becke, *J. Chem. Phys.*, 1997, **107**, 8554–8560.

5 A. D. Becke, *Phys. Rev. A*, 1988, **38**, 3098.

6 F. Rezaie and S. Noorizadeh, *Dalt. Trans.*, 2023, **52**, 12562–12563.

7 X. Li, S. Yang, M. Liu, S. Liu, Q. Miao, Z. Duan, P. Qiao, J. Lin, F. Sun, Q. Xu and Z. Jiang, *Small Struct.*, 2023, **4**, 2200320.

8 S. K. Das, G. Kumar, M. Das and R. S. Dey, *Mater. Today Proc.*, 2022, **57**, 228–233.

9 J. Y. Yue, Y. T. Wang, X. Wu, P. Yang, Y. Ma, X. H. Liu and B. Tang, *Chem. Commun.*, 2021, **57**, 12619–12622.

10 X. Yu, Y. Ma, C. Li, X. Guan, Q. Fang and S. Qiu, *Chem. Res. Chinese Univ.*, 2022, **38**, 167–172.

11 D. Li, C. Li, L. Zhang, H. Li, L. Zhu, D. Yang, Q. Fang, S. Qiu and X. Yao, *J. Am. Chem. Soc.*, 2020, **142**, 8104–8108.

12 J. Guo, C. Y. Lin, Z. Xia and Z. Xiang, *Angew. Chemie Int. Ed.*, 2018, **57**, 12567–12572.

13 S. Roy, S. Mari, M. K. Sai, S. C. Sarma, S. Sarkar and S. C. Peter, *Nanoscale*, 2020, **12**, 22718–22734.

14 S. Royuela, E. Martínez-Periñán, M. P. Arrieta, J. I. Martínez, M. M. Ramos, F. Zamora, E. Lorenzo and J. L. Segura, *Chem. Commun.*, 2020, **56**, 1267–1270.

15 T. Boruah, S. K. Das, G. Kumar, S. Mondal and R. S. Dey, *Chem. Commun.*, 2022, **58**, 5506–5509.

16 S. Yang, Q. Xu, P. Qiao, J. Liu, X. Chen, Z. Tian, N. Zhang, S. H. Kim, S. Lu, X. Liu, X. Li and Z. Jiang, *Mater. Today Chem.*, 2022, **24**, 100936.

17 S. Chang, C. Li, H. Li, L. Zhu and Q. Fang, *Chem. Res. Chinese Univ.*, 2022, **38**, 396–401.

18 P. García-Arroyo, E. Martínez-Periñán, J. J. Cabrera-Trujillo, E. Salagre, E. G. Michel, J. I. Martínez, E. Lorenzo and J. L. Segura, *Nano Res.*, 2022, **15**, 3907–3912.

19 Z. You, B. Wang, Z. Zhao, Q. Zhang, W. Song, C. Zhang, X. Long, Y. Xia, Z. You, B. Wang, Z. Zhao, Q. Zhang, W. Song, C. Zhang, X. Long and Y. Xia, *Adv. Mater.*, 2023, **35**, 2209129.

20 G. Henkelman, L. Wei, Y. Chen, C. Liu, F. Liu, H. Li, J. Chen, J. Fei, Z. Yu, Z. Yuan, C. Wang, H. Zheng, Z. Liu and M. Xu, *ACS Nano*, 2021, **15**, 3309–3319.

21 J. Jia, J. Li, S. Ma, Z. Zhang and X. Liu, *Macromol. Rapid Commun.*, 2023, **44**, 2200717.

22 J. Liu, Y. Hu and J. Cao, *Catal. Commun.*, 2015, **66**, 91–94.

23 X. Yan, B. Wang, J. Ren, X. Long and D. Yang, *Angew. Chemie*, 2022, **134**, e202209583.